

ICP
Heavy Metal Contamination in
Pet Food: Changes Over a Decade

THEORY & FUNDAMENTALS
Raman and Photoluminescence
Imaging of Two-Dimensional WS₂

TECHNIQUE FOCUS
Our 2021 Employment
and Salary Survey

MARCH 2021
VOLUME 36 | NO. 3

Spectroscopy[®]

SOLUTIONS FOR MATERIALS ANALYSIS



APPLICATIONS

**Raman and Mid-IR
Discrimination of
Geographical Origin
of Rice**

RAMAN

**Mixture Solution Analysis
Using Silver Nanoparticles
and SERS**

IR

**An Introduction to
Infrared Spectral
Library Searching**

SPECTROSCOPYONLINE.com

Accurate, Affordable NIR Analysis

Ocean Insight offers NIR spectrometers that meet price and performance criteria at every level. What's the best model for your application?

- High-sensitivity **NIRQuest+** spectrometers for measurements from 900-2500 nm



- **NanoQuest** MEMS-based device (1350-2500 nm) that's smaller than your smartphone

- **Flame-NIR+** miniature spectrometer with remarkable response from 970-1700 nm



Visit [OceanInsight.com](https://www.oceaninsight.com) today for details on two great NIR spectrometer promotions!

KnowItAll Spectral Software & Libraries

IDENTIFY SPECTRA

IR MS RAMAN NMR UV-VIS



KnowItAll combines the world's largest spectral database with powerful analytical tools for fast, accurate results!

GET TRIAL
knowitall.com/trial

sciencesolutions.wiley.com

WILEY

MANUSCRIPTS: To discuss possible article topics or obtain manuscript preparation guidelines, contact the editorial director at: (732) 346-3020, e-mail: LBush@mmhgroup.com. Publishers assume no responsibility for safety of artwork, photographs, or manuscripts. Every caution is taken to ensure accuracy, but publishers cannot accept responsibility for the information supplied herein or for any opinion expressed.

SUBSCRIPTIONS: For subscription information: *Spectroscopy*, P.O. Box 457, Cranbury, NJ 08512-0457; email mmhinfo@mmhgroup.com. Delivery of *Spectroscopy* outside the U.S. is 3–14 days after printing.

CHANGE OF ADDRESS: Send change of address to *Spectroscopy*, P.O. Box 457, Cranbury, NJ 08512-0457; provide old mailing label as well as new address; include ZIP or postal code. Allow 4–6 weeks for change. Alternately, go to the following URL for address changes or subscription renewal: <http://mmhpubs.mmhgroup.com/Welcomes.aspx?pubid=SPEC>

C.A.S.T. DATA AND LIST INFORMATION: Contact Melissa Stillwell, (218) 740-6831; e-mail: MStillwell@mmhgroup.com

Reprints: Contact Stephanie Shaffer, e-mail: SShaffer@mjlhifesciences.com

INTERNATIONAL LICENSING: Contact Kim Scaffidi, e-mail: KScaffidi@mjlhifesciences.com

CUSTOMER INQUIRIES: Customer inquiries can be forwarded directly to MJH Life Sciences, Attn: Subscriptions, 2 Clarke Drive, Suite 100, Cranbury, NJ 08512; e-mail: mmhinfo@mmhgroup.com



© 2020 MultiMedia Pharma Sciences, LLC. All rights reserved. No part of this publication may be reproduced or transmitted in any form or by any means, electronic or mechanical including by photocopy, recording, or information storage and retrieval without permission in writing from the publisher. Authorization to photocopy items for internal/educational or personal use, or the internal/educational or personal use of specific clients is granted by MultiMedia Pharma Sciences, LLC. for libraries and other users registered with the Copyright Clearance Center, 222 Rosewood Dr. Danvers, MA 01923, (978) 750-8400, fax (978) 646-8700, or visit <http://www.copyright.com> online. For uses beyond those listed above, please direct your written request to Permission Dept. email: ARockenstein@mjlhifesciences.com

MultiMedia Pharma Sciences, LLC. provides certain customer contact data (such as customer's name, addresses, phone numbers, and e-mail addresses) to third parties who wish to promote relevant products, services, and other opportunities that may be of interest to you. If you do not want MultiMedia Pharma Sciences, LLC. to make your contact information available to third parties for marketing purposes, simply email mmhinfo@mmhgroup.com and a customer service representative will assist you in removing your name from MultiMedia Pharma Sciences, LLC. lists.

Spectroscopy does not verify any claims or other information appearing in any of the advertisements contained in the publication, and cannot take responsibility for any losses or other damages incurred by readers in reliance of such content.

To subscribe, email mmhinfo@mmhgroup.com.

AN **MH** life sciences™ BRAND

485F US Highway One South,
Suite 210
Iselin, NJ 08830
(732) 596-0276
Fax: (732) 647-1235

PUBLISHING/SALES

**Senior Vice President,
Industry Sciences**
Michael J. Tessalone
MTessalone@mjlhifesciences.com

Group Publisher
Stephanie Shaffer
SShaffer@mmhgroup.com

Associate Publisher
Edward Fantuzzi
EFantuzzi@mjlhifesciences.com

Account Executive
Timothy Edson
TEdson@mjhassoc.com

Account Executive
Michael Howell
MHowell@mjlhifesciences.com

Senior Director, Digital Media
Michael Kushner
MKushner@mjlhifesciences.com

EDITORIAL

Editorial Director
Laura Bush
LBush@mjlhifesciences.com

Managing Editor
John Chasse
JChasse@mjlhifesciences.com

Senior Technical Editor
Jerome Workman
JWorkman@mjlhifesciences.com

Associate Editor
Cindy Delonas
CDelonas@mjlhifesciences.com

Assistant Editor
Will Wetzel
WWetzel@mjlhifesciences.com

Creative Director, Publishing
Melissa Feinen
MFeinen@mdmag.com

Senior Art Director
Gwendolyn Salas
GSalas@mjlhifesciences.com

Senior Graphic Designer
Courtney Soden
CSoden@mjlhifesciences.com

CONTENT MARKETING

Custom Content Writer
Alissa Marrapodi
AMarrapodi@mjlhifesciences.com

Webcast Operations Manager
Kristen Moore
KMoore@mjlhifesciences.com

Project Manager
Vania Oliveira
VOliveira@mmhgroup.com

Digital Production Manager
Sabina Advani
SAdvani@mjlhifesciences.com

**Managing Editor,
Special Projects**
Kaylynn Chiarello-Ebner
KEbner@mjlhifesciences.com

MARKETING/OPERATIONS

Marketing Manager
Brianna Pangaro
BPangaro@mjlhifesciences.com

**C.A.S.T. Data and
List Information**
Melissa Stillwell
MStillwell@mmhgroup.com

Reprints
Alexandra Rockenstein
ARockenstein@mjlhifesciences.com

Audience Development Manager
Jessica Stariha
JStariha@mmhgroup.com

CORPORATE

Chairman & Founder
Mike Hennessy Sr

Vice Chairman
Jack Lepping

President & CEO
Mike Hennessy Jr

Chief Financial Officer
Neil Glasser, CPA/CFE

Chief Marketing Officer
Michael Baer

**Executive Vice President,
Global Medical Affairs &
Corporate Development**
Joe Petroziello

**Senior Vice President,
Content**
Silas Inman

**Senior Vice President,
Operations**
Michael Ball

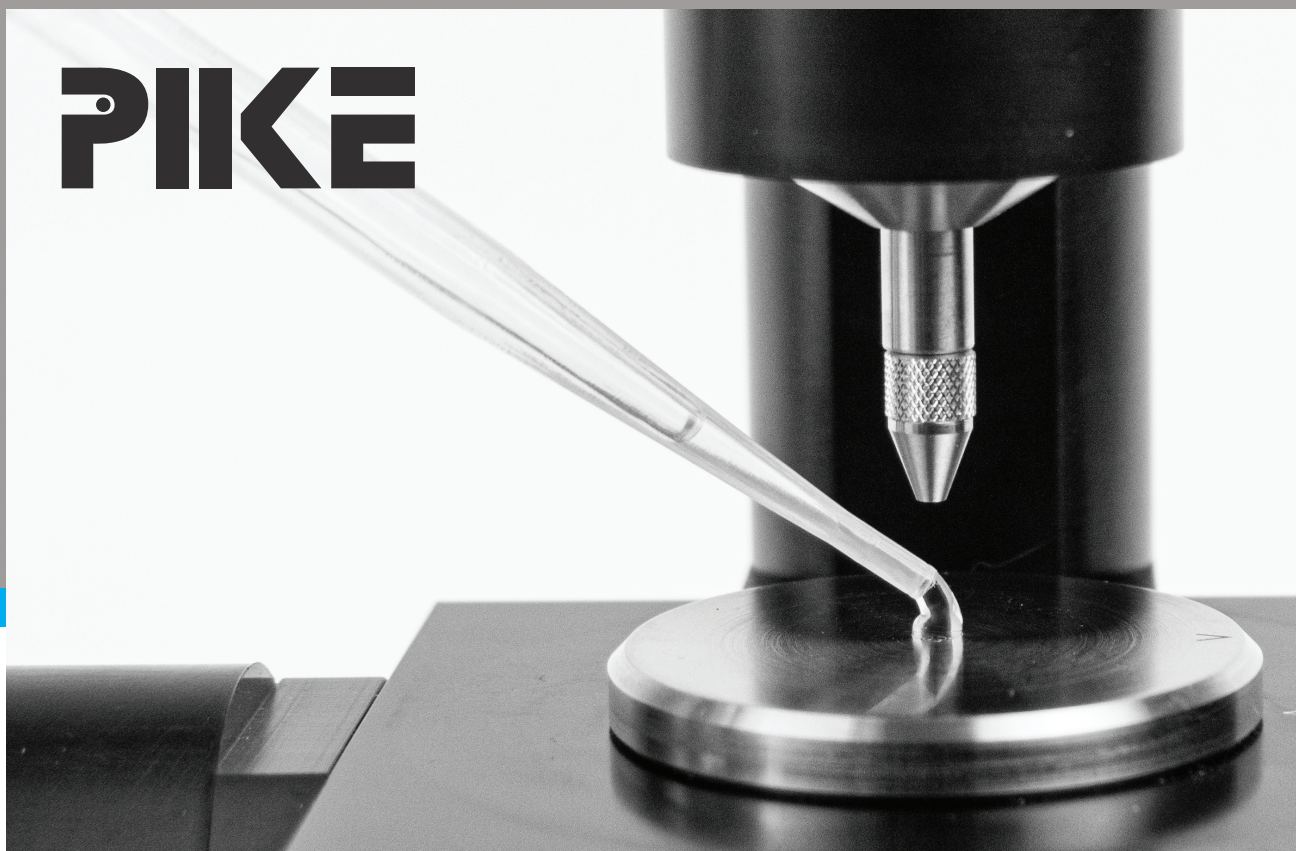
**Senior Vice President,
I.T. & Enterprise Systems**
John Moricone

**Vice President, Human
Resources & Administration**
Shari Lundenberg

**Vice President,
Mergers & Acquisitions**
Chris Hennessy

**Executive Creative Director,
Creative Services**
Jeff Brown

PIKE



The IRIS DIAMOND ATR

PRECISION OPTICS FOR HIGH ENERGY THROUGHPUT.

Generate high-quality spectra with IRIS. You can measure a wide range of samples including powders, gels, liquids and solids. Ideal for research, QA/QC and sample identification.



TABLE OF CONTENTS

March 2021

Volume 36 | Number 3

COLUMNS

- 9 Molecular Spectroscopy Workbench**
Combined Raman and Photoluminescence Imaging of Two-Dimensional WS₂
David Tuschel
Raman and photoluminescence spectroscopy were combined with imaging to examine the spatial variation of solid-state structure and electronic character of two-dimensional (2-D) tungsten disulfide (WS₂) crystals, which represent a family of new inorganic 2-D materials.
- 13 Atomic Perspectives**
Heavy Metals in Pet Food: Changes in Heavy Metal Contamination in Pet Food Over the Past Decade
Patti Atkins, Tina Restivo, and Bob Lockerman
Analysis of heavy metals in pet food using ICP-OES was conducted to determine if there were potentially toxic elements present. Many of the samples showed significant concentrations of various toxic metals.
- 24 IR Spectral Interpretation Workshop**
Library Searching
Brian C. Smith
One of the biggest practical limitations of infrared spectroscopy is its difficulty in analyzing mixtures. Infrared library searching can help, but it must be done right.

FEATURED ARTICLE

- 44 The 2021 Employment and Salary Survey: Covid-19 and the New Virtual World**
Jerome Workman, Jr.
We report on overall salary trends and how they compare to past years. We also look beyond the numbers to focus on broader trends of workplace satisfaction and career attitudes for spectroscopists.

PEER-REVIEWED RESEARCH

- 28 Analysis of a Mixture Solution Using Silver Nanoparticles Based on Surface-Enhanced Raman Spectroscopy (SERS)**
Lin Bao, Siqingaowa Han, and Wuliji Hasi
SERS can be used for the detection and monitoring of drugs as pure compounds and mixtures. A demonstration of a sample preparation method used to detect components with weak substrate adsorption in the spectrum of a mixed solution is shown.
- 34 Enhanced Raman and Mid-Infrared Spectroscopic Discrimination of Geographical Origin of Rice by Data Mining and Data Fusion**
Min Sha, Dongdong Gui, Peng Li, Zhengyong Zhang, Yu Huang, Minqin Jiang, and Jun Liu
The application of data mining combined with data fusion of Raman and mid-infrared spectra was studied to improve discrimination ability for modeling the geographical origins of rice.



Cover art: Closeup of organic green paddy rice field prepared for autumn harvest

DEPARTMENTS

Products	49
Ad Index	50

- Like @SpectroscopyMagazine on Facebook
- Follow @SpectroscopyMag on Twitter
- Join the Group @SpecGroup on LinkedIn



MB3000-CH90 laboratory gas analyzer

Measurement made easy

The MB3000-CH90 gas analyzer provides fast and accurate FT-IR critical gas measurements down to ppb levels in a user-friendly environment. This high performance and maintenance-free spectrometer is used in R&D or QA/QC laboratories for checking gas purity, controlling gas mixing and composition or performing unknown components speciation. The heated gas cell can be easily swapped and replaced with other sampling accessories, making the MB3000-CH90 a flexible and versatile tool for any laboratory.

Measurement made easy.

Want to learn more? Visit abb.com/analytical
or contact us at ftir@ca.abb.com

ABB

EDITORIAL ADVISORY BOARD

Fran Adar Horiba Scientific

Russ Algar University of British Columbia

Matthew J. Baker University of Strathclyde

Ramon M. Barnes University of Massachusetts

Matthieu Baudelet University of Central Florida

Rohit Bhargava University of Illinois at Urbana-Champaign

Karl S. Booksh University of Delaware

Michael S. Bradley Thermo Fisher Scientific

Deborah Bradshaw Consultant

Lora L. Brehm The Dow Chemical Company

George Chan Lawrence Berkeley National Laboratory

John Coates Coates Consulting LLC

John Cottle University of California Santa Barbara

Paul J. Gemperline East Carolina University

David Lankin University of Illinois at Chicago, College of Pharmacy

Barbara S. Larsen DuPont Nutrition and Biosciences

Barry K. Lavine Oklahoma State University

Igor K. Lednev University at Albany, State University of New York

Bernhard Lendl Vienna University of Technology (TU Wien)

Ian R. Lewis Kaiser Optical Systems

Howard Mark Mark Electronics

R.D. McDowall McDowall Consulting

Gary McGeorge Bristol-Myers Squibb

Francis M. Mirabella Jr. Mirabella Practical Consulting Solutions, Inc.

Ellen V. Miseo TeakOrigin

Michael L. Myrick University of South Carolina

John W. Olesik The Ohio State University

Yukihiro Ozaki Kwansei Gakuin University

Steven Ray State University of New York at Buffalo

Jim Rydzak Specere Consulting


Jacob T. Shelley Rensselaer Polytechnic Institute

Barry Wise Eigenvector Research Inc.


Jerome Workman Jr. Biotechnology Business Associates

Lu Yang National Research Council Canada

Spectroscopy's Editorial Advisory Board is a group of distinguished individuals assembled to help the publication fulfill its editorial mission to promote the effective use of spectroscopic technology as a practical research and measurement tool. With recognized expertise in a wide range of technique and application areas, board members perform a range of functions, such as reviewing manuscripts, suggesting authors and topics for coverage, and providing the editor with general direction and feedback. We are indebted to these scientists for their contributions to the publication and to the spectroscopy community as a whole.



Next generation Raman imaging



High performance Raman systems for a range of applications

Raman spectroscopy produces chemical and structural images to help you understand more about the material being analyzed. Renishaw has decades of experience developing flexible Raman systems that give reliable results, for even the most challenging measurements. With Renishaw's suite of Raman systems, you can see the small things, the large things and things you didn't even know were there.

Visit www.renishaw.com/raman

Renishaw, Inc. 1001 Wesemann Drive, West Dundee, Illinois, 60118, United States
T +1 847 286 9953 F +1 847 286 9974 E raman@renishaw.com
www.renishaw.com

Combined Raman and Photoluminescence Imaging of Two-Dimensional WS₂

David Tuschel

Combined Raman and photoluminescence (PL) spectroscopy and imaging are used to examine the spatial variation of solid-state structure and electronic character of two-dimensional (2-D) tungsten disulfide (WS₂) crystals. Simultaneous mapping acquisition of PL and Raman scattering from the same spatial locations provide complementary structural information and a way of rendering combinative Raman and PL spectral images of thin film 2-D crystals in general, and WS₂ in particular.

Graphene is probably the most well-known of the emerging class of materials known as two-dimensional (2-D) crystals. These materials are constituted by monolayer to few-layered structures. In recent years, new inorganic 2-D materials have emerged, including MoS₂, MoSe₂, WS₂, and WSe₂, among others. These materials have attracted significant interest because of their special electronic, optical, and optoelectronic properties in the monolayer to few-layer forms that are different from those of the bulk form (1,2). One of the most significant differences of the 2-D crystals is the transformation from an indirect band gap semiconductor in the bulk to a direct band gap semiconductor in the monolayer to few-layer crystals. Thus, the fabrication of optoelectronic devices in addition to familiar integrated electronic circuitry is envisioned for these materials. These optoelectronic characteristics have prompted substantial research to discover the means of fabrication and the physical characteristics of 2-D crystals to produce integrated electronic and optoelectronic devices (3).

Raman and Photoluminescence (PL) Imaging of 2-D WS₂

You may have observed the spatially varying colors in reflected white light images of 2-D crystals, and so there have been developments to use optical microscopy to rapidly identify the number of molecular layers that make up the 2-D crystal (4). Previously, we reported on the use of Raman and PL spectroscopy and imaging of few-layer MoS₂ to identify spatial variation in the number of layers and strain (5–7). In this installment of “Molecular Spectroscopy Workbench,” we focus on combined Raman and PL imaging for the characterization of 2-D WS₂ crystals.

Here, we apply Raman and PL spectral imaging to reveal the spatially varying structural differences that are not observed when viewing the crystals with reflected white light microscopy. A collection of hyperspectral data acquired by spectral mapping of a 2-D WS₂ crystal is shown in Figure 1. A reflected white light image of the crystal appears in the lower right-hand corner, and a combinative Raman and photoluminescence image corresponding to the reflected light image appears to its left. The plot on the upper left

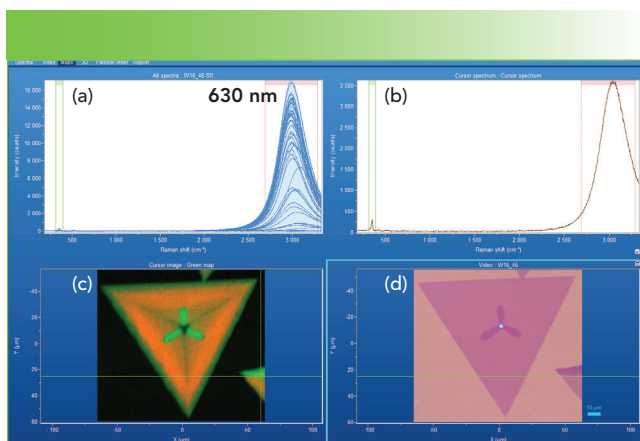


FIGURE 1: (a) hyperspectral data set, (b) cursor spectrum, (c) combinative Raman and photoluminescence image, and (d) reflected white light image of 2-D WS₂ crystal.

consists of all the spectra acquired over the image area, and the upper right-hand plot shows the single spectrum associated with the cross-hair location in the spectral and reflected light images. Note that each spectrum covers a spectral range that includes contributions from both Raman scattering and PL. The Raman and PL data

were acquired using 532 nm excitation in conjunction with a 300 gr/mm grating and a 50x Olympus objective and by moving the stage in 1.5 μm increments over an area of approximately 100 μm x 100 μm. The combinative spectral image is rendered through a color-coded plot of the spatial variation of Raman (green) and PL (red) signal strength within the corresponding color bracketed Raman shift positions shown in the two upper traces. The combinative Raman and PL image is actually a rendering of normalized (minimum to maximum) signal strength for the Raman band at 349 cm⁻¹ and the PL band centered primarily at 630 nm as a function of position on the sample. The hyperspectral data clearly reveal the nonuniformity of the PL corresponding to a spatial variation of the intensity and peak position. Consequently, PL images could be rendered of the spatially varying peak position along with that of spatially varying signal strength.

The triangular crystal consists primarily of a single layer of WS₂ with a three-pronged two-layer formation growing out from the center. The light blue triangle in the center of the reflected white light image consists of multiple layers of WS₂. The three-pronged two-layer formation appears darker purple in the reflected white light image and brighter green in the combinative Raman and PL spectral image, because of the greater Raman scattering and attenuated PL from the two-layer structure. The combinative spectral image is rendered through a color-coded plot of Raman (green) and PL (red) signal strength where each component's color intensity scale is normalized minimum to maximum to reveal the spatially varying contrast of both spectral components. Were the color intensities to be plotted on the same absolute scale and not normalized, the image would essentially consist of only the PL contribution because of the weak Raman scattering strength relative to that of the far more intense PL.

The separate Raman and PL images in Figure 2 show the spatially varying differences in solid state structure as revealed through vibrational and electronic spectroscopy, respectively. The three-pronged two-layer formation appears brighter in the Raman image than the rest of the single-layer crystal, which appears uniform and dark green. The triangular feature in the center appears dark, consistent with all past reporting that many layer structures have been shown to generate much weaker Raman scattering than either single or few-layer 2-D crystals.

In contrast with the Raman image, the three-pronged two-layer formation appears dark in the PL image because of very weak emission. The diminished PL in the surrounding single-layer area grows progressively brighter towards the crystal perimeter. Furthermore, dark lines indicating attenuated PL in the

Quality Cells for Quality results

Fully fused construction
Transmission from 190 nm to 3800 nm
Path lengths from 0.008 to 500 mm
Volumes from 0.5μl to 170ml
Wide range of standard cells
Custom designs

Starna
Starna Scientific Ltd

Starna Cells Inc.
(800) 228-4482
sales@starnacells.com
www.starna.com

single-layer area bisect the three prongs of the two-layer formation. One can envision a triangle formed by lines perpendicular to the tips of the three two-layer prongs. A spatial variation of attenuated PL appears within that triangle. Outside of that triangle boundary, the PL is uniformly strong. Nevertheless, the most striking contrast in the PL image appears because the two-layer formation yields very weak PL emission relative to that of the single-layer portion. Also, note that the large triangle in the PL image is smaller than that of the Raman image. That is because the PL is attenuated at the perimeter of the crystal. When these two images are overlaid with normalized intensities, one obtains the combinative Raman and PL image shown in Figure 2c. The contrasting colors are the result of the spatially varying relative contributions of the Raman and PL signals. Moreover, the Raman and PL signal strengths are each normalized (minimum to maximum). That is why the perimeter of the crystal appears green from strong Raman scattering and because of the absence of or significantly attenuated PL at that location relative to the interior of the single-layer formation.

A second set of Raman, PL, combinative Raman and PL, and reflected white light images from another WS_2 crystal is shown in Figure 3. This crystal consists entirely of two single-layers of WS_2 that have grown into each other. Consequently, the Raman image in Figure 3a appears almost entirely uniform except for the dim line at the interface of the crystal growth and the small dark spot at the center that spatially corresponds to the spot in the center of the reflected white light image. That small spot takes on significance in the PL image of Figure 3b that appears dark and slightly larger than that in the Raman and reflected white light images. Furthermore, dark lines of attenuated PL propagate from the center spot to each

of the corners of the two crystals in a manner similar to that observed in the single crystal of Figure 2b. The contrast between the uniformity and spatial variations of the Raman and PL images, respectively is striking. When these two images are overlaid with normalized intensities, one obtains the combinative Raman and PL image shown in Figure 3c.

Here, the minimum-to-maximum color contrast generates a green-yellow combinative Raman and PL image, whereas that of Figure 2c is green-orange. The reason for this difference in color contrast is because of the normalized intensity color scaling. The Raman image of Figure 3a is of nearly uniform intensity, thereby generating a uniformly



Take Control of Your Analysis

All labs have their challenges—slow analysis times, unreliable instrumentation, and unsure results. At LECO we lead the way to dependable results by working with you to provide a solution to these challenges. Today's innovative solutions for materials characterization and elemental analysis reflect our commitment to improving your lab's overall productivity and efficiency.



GDS900 Glow Discharge Atomic Emission Spectrometer
High performance bulk elemental analysis of metals and other solid conductive materials.

Phone: 1-800-292-6141 | info@leco.com
www.leco.com | © 2021 LECO Corporation

LECO
EMPOWERING RESULTS

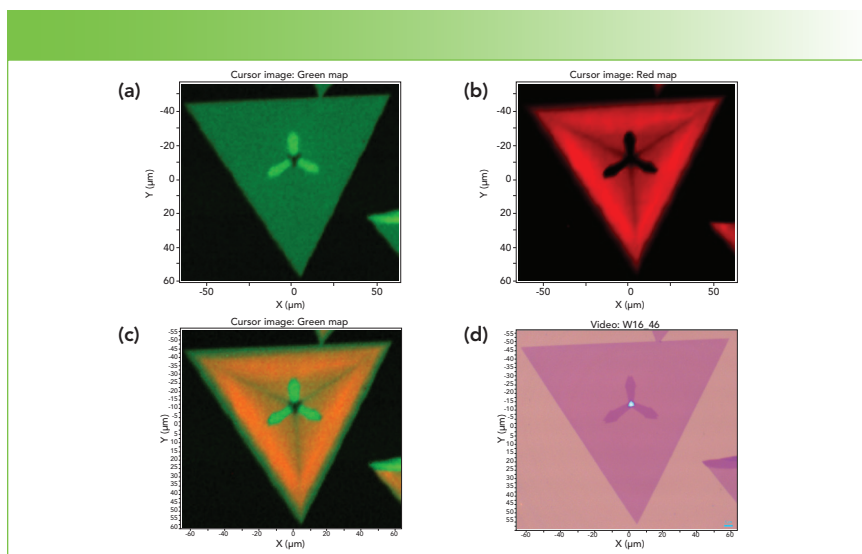


FIGURE 2: Spectral and reflected white light imaging of WS_2 : (a) Raman, (b) photoluminescence, (c) combinative Raman and photoluminescence, and (d) reflected white light image.

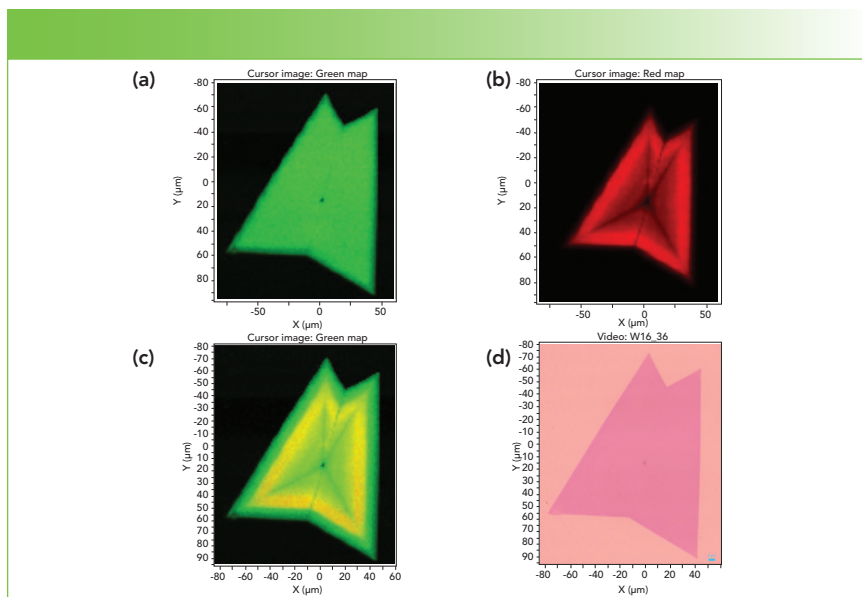


FIGURE 3: Spectral and reflected white light imaging of WS_2 : (a) Raman, (b) photoluminescence, (c) combinative Raman and photoluminescence, and (d) reflected white light image.

flat green Raman background for the combinative Raman and PL image. However, the Raman image of Figure 2a has spatially varying intensity because of the presence of both single and two-layer structures. Consequently, the relative Raman signal contribution under the single-layer formation contributes less than under the three two-layer prongs in the combinative Raman and

PL image of Figure 2c. The normalized PL signal in Figure 2c is relatively stronger than that of the Raman scattering of the single-layer formation resulting in the orange color in the combinative Raman and PL image. Such color contrasts demonstrate the effectiveness of combined imaging to reveal the relative Raman to PL signal strengths in different crystals.

Conclusion

Raman and PL spectroscopy reveal different aspects of the solid-state structure of 2-D materials. Combined Raman and PL imaging performed simultaneously with one instrument reveals the spatial variation of the solid-state structure and electronic properties of 2-D crystals that is not revealed in reflected white light imaging. Furthermore, examples of combinative Raman and PL images of WS_2 crystals reveal the variation of Raman to PL signal strengths within and among different crystals. The ability to image crystals through vibrational and electronic spectroscopy should allow materials scientists to better design and fabricate electronic and optoelectronic devices based upon 2-D crystals.

References

- (1) D. Jariwala, V.K. Sangwan, L.J. Lauhon, T.J. Marks and M.C. Hersam, *ACS Nano*. **8**, 1102–1120 (2014).
- (2) G. Eda and S.A. Maier, *ACS Nano*. **7**, 5660–5665 (2013).
- (3) R. Ganatra and Q. Zhang, *ACS Nano*. **8**, 4074–4099 (2014).
- (4) H. Li, J. Wu, X. Huang, G. Lu, J. Yang, X. Lu, Q. Xiong and H. Zhang, *ACS Nano*. **7**, 10344–10353 (2013).
- (5) D. Tuschel, *Spectroscopy* **30**(3), 14–29 (2015).
- (6) D. Tuschel, *Spectroscopy* **34**(9), 10–21 (2019).
- (7) D. Tuschel, *Spectroscopy* **35**(3), 9–16 (2020).



David Tuschel is a Raman Applications Scientist at Horiba Scientific, in Piscataway, New Jersey, where he works with Fran Adar. David is sharing authorship of this column with Fran. He can be reached at: SpectroscopyEdit@MMHGroup.com •

Heavy Metals in Pet Food: Changes in Heavy Metal Contamination in Pet Food Over the Past Decade

Patti Atkins, Tina Restivo, and Bob Lockerman

Pet food is a multibillion dollar per year business that affects businesses and pet owners on a daily basis. Along with increased growth, there has been increased controversy. The melamine pet food scare of 2007 affected millions of people and their pets, along with the pet food industry. The pet food scare highlighted the potential for contaminants and controversial ingredients that could be contained in pet food. In addition to organic chemical contaminants and additives, there is also the possibility of toxic elemental contamination from protein sources, fillers, and manufacturing processes. Therefore, the search for “healthy” pet food goes beyond the choice of a name brand food or nutritious ingredients on a label.

Ten years ago, SPEX CertiPrep, first introduced its popular study on “Heavy Metals in Pet Food,” which was featured in *Spectroscopy* (1,2). The purpose of this 2009 study was to examine pet foods from a variety of sources to determine if there were potentially toxic elements present in the foods. Many of the pet foods sampled showed significant concentrations of various toxic metals. In many cases, the concentrations exceeded the extrapolated human limit values calculated to pet-size dosages.

In the intervening 10 years, the Food Safety Modernization Act (FSMA) was enacted, and pet food became one of the targets of scrutiny. This new 2019 study was produced as a joint effort between SPEX companies and CEM Corporation, and revisits pet food brands first analyzed in 2009, while looking at new brands that have emerged after the 2007 pet food crisis and later enactment of the FSMA, to determine whether heavy metal contamination has significantly changed in the decade following the first study. Using updated cryogenic and microwave technologies, samples were tested by inductively coupled plasma (ICP) and inductively coupled plasma–mass spectrometry (ICP–MS) to determine heavy metal content, and

these results were compared to our previous 2009 study.

Recently, I presented a summary of our findings in an interview for *Spectroscopy* (3). The purpose of this article is to expand on those findings.

History

Some of the first commercial dog food has been credited to a businessman in the 1860s who developed a dog biscuit after he witnessed dogs being fed leftover hardtack biscuits in the ports of England. His idea later came to the United States in the late 1890s, but the canned pet food we know today did not exist extensively until after World War I (WWI). Ken-L-Ration brand (1922) was the first commercial pet food sold because of an excess of horse meat after WWI. In the early part of the 20th century, the U.S. Food and Drug Administration (FDA) did not exist, and only human food and medicine was under consideration of the 1906 Pure Food and Drug Act.

The first controls of pet food came under the 1938 Federal Food, Drug, and Cosmetic Act, which only required that pet food be safe to eat, produced under sanitary conditions, free from harmful substances, and labelled truthfully as to its quantity, identity,

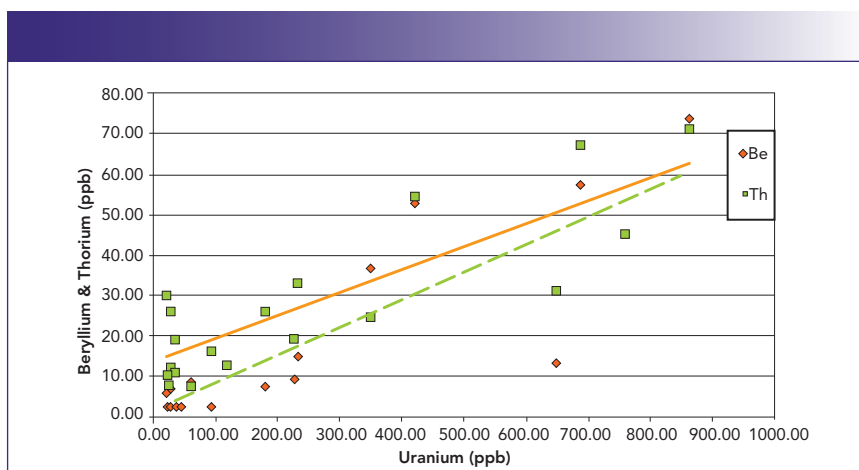


FIGURE 1: A 2009 comparison: uranium vs. beryllium and thorium.

TABLE I: Cryogenic grinding mill operating conditions for dry pet food

Parameter	Value
Precooling time	5 min
Grinding time	2 min
Cooling time	1 min
Number of cycles	3
Rate or frequency	12 Hz

TABLE II: Comparison of concentration of toxic metals 2009 and 2019

Element	2009 Pet Food Min (ppb)	2019 Pet Food Min (ppb)	2009 Pet Food Max (ppb)	2019 Pet Food Max (ppb)
Al	300	390	215000	86302
As	4	20	290	687
Be	2	ND	74	114
Cd	2	ND	130	152
Co	23	70	920	1343
Cr	15	397	2500	34191
Hg	ND	Not reported	55	Not reported
Ni	48	354	3200	5879
Pb	3	16	5900	515
Sb	1	ND	970	318
Se	64	190	1500	1068
Sn	6	ND	9400	143
Th	ND	ND	90	147
Tl	1	ND	10	28
U	ND	ND	860	1699
V	5	43	7400	3339

manufacturing process, ingredients (listed by weight), and nutritional information. The next significant advance of pet food also came after a major war when the consumer canned and packaged food companies that grew out of war rations, then transitioned to a post war economy. These companies capitalized on the ability to use human food by-products to create pet food.

Extruded dry kibble began to appear in the mid-1950s, and the pet food industry flourished and became mainstream, ultimately growing into a multibillion dollar a year global industry. The 1960s saw increases in specialized pet foods and an increase in brands and product lines for established companies. The first big public scare in the pet food industry started with the 2007 discovery of melamine and cyanuric acid in a wide range of pet food varieties and brands. Early in 2007, there were hundreds of pet deaths and illnesses because of kidney failure around the world, which was later traced back to illegal protein adulteration. Chinese raw material manufacturers had added the melamine to the pet food to artificially increase the protein content. Over 5000 product recalls were announced across multiple brands, manufacturers, and suppliers, linked to almost 10,000 pet deaths and illnesses.

2009 Heavy Metals Study

For years after the melamine pet food disaster, pet owners continued to be concerned about their pet's food. The initial disaster happened because of terrible oversight of supply chains and lack of testing for harmful ingredients. The pet food industry claimed that, as a result of the melamine scare, there was more active policing in their industry and products, but questions still remained whether pet food was safe or not. In 2009, SPEX CertiPrep made a decision to look at the elemental content of pet food. SPEX CertiPrep was a close-knit family company whose employees and owners were dedicated pet owners. The study solicited pet food from

MARS 6™

Microwave Digestion System

Rapid, safe, and easy-to-use for all your critical metals analysis needs.



More pets trust MARS 6 for their sample prep than any other microwave digestion system in the world.

Visit us at cem.com



We Simplify Science

© 2021 CEM Corporation. All Rights Reserved.

TABLE III: Reference dosages (RfD) and tolerable daily intake (TDI) calculated for a 50 pound (lb.) dog.

Element	EPA Human RfD ($\mu\text{g}/\text{kg}/\text{day}$)	EPA Human RfD (Per 50 lbs. Body Weight)	WHO Human TDI ($\mu\text{g}/\text{kg}/\text{day}$)	WHO Human TDI (Per 50 lbs. Body Weight)
As	0.3	7	2.14	49
Be	2	45	-	-
Cd	1	23	1	23
Ni	20	454	12	272
Pb	-	-	3.6	82
Sb	0.4	9	6	136
Tl	0.1	2.3	-	-
U	3	68	0.6	14

TABLE IV: Reference dosages (RfD) and tolerable daily intake (TDI) for a 10 pound (lb.) cat

Cat Limit	EPA Human RfD ($\mu\text{g}/\text{kg}/\text{day}$)	EPA Human RfD (Per 10 lbs. Body Weight)	WHO Human TDI ($\mu\text{g}/\text{kg}/\text{day}$)	WHO Human TDI (Per 10 lbs. Body Weight)
As	0.3	1.4	2.14	9.72
Be	2	9	-	-
Cd	1	4.5	1	4.5
Ni	20	91	12	55
Pb	-	-	3.6	16
Sb	0.4	1.8	6	27
Tl	0.1	0.5	-	-
U	3	14	0.6	2.7

all the employees, and purchased food from local pet stores, groceries, dollar stores, and supercenters. We decided to investigate all price ranges, from the cheapest dollar store food to the boutique gourmet brands sold in specialty markets. The original study was conducted in the winter of 2009–2010, covering almost sixty samples. The samples included approximately equal amounts of cat and dog foods, as well as equal amounts of wet canned food and dry kibble.

Once the foods had been grounded, digested, and tested, it was found that there were substantially high amounts (up to ppm levels) of heavy metals and wear metals (from the processing equipment) in pet food, especially in dry kibbles. The amount of food that

owners fed their pets increased the exposure of pets to higher levels of potentially toxic metals. Despite the fact that pet food had been under the control of the FDA since 1938, there was no guidance in 2009 regarding the limits for the most toxic elements to dogs and cats. Instead, the SPEX CertiPrep study used human exposure guidelines issued by the EPA and scaled them to a standardized size (50 lbs for a dog and 10 lbs for a cat).

In the decade since the first heavy metals study, the FSMA was created. Pet food fell under the direction of the FDA within the FSMA, and it was our hope that public awareness of the previous pet food regulatory shortfalls would be corrected and lower metal content would now be seen in pet food.

Experimental

The basic techniques, materials, and methods for both the 2009 and 2019 studies were similar. Differences in the studies included the use of updated equipment and instrumentation, which will be discussed within the “Methods” section. For details on the previous 2009 experimental conditions, please refer to the originally published articles published in *Spectroscopy* in 2011 (1,2).

Reagents and Standards

In both the 2009 and 2019 studies, concentrated optima-grade nitric acid was obtained from Fisher Scientific. Deionized water was obtained from an in-house laboratory water filtration and processing system, which produces deionized water (ASTM I grade).

The SPEX CertiPrep standards (SPEX CertiPrep Group) used in both studies included:

- CLMS-2N: Claritas Multielement Solution Standard
- (10 mg/L: Ag, Al, As, Ba, Be, Bi, Ca, Cd, Co, Cr, Cs, Cu, Fe, Ga, In, K, Li, Mg, Mn, Na, Ni, Pb, Rb, Se, Sr, Tl, U, V, and Zn)
- CL-ICV-1: Claritas Initial Calibration Verification 1
- (1000 mg/L: Fe, K, Ca, Na, Mg, Sr; 10 mg/L: Ag, Al, As, Ba, Be, Cd, Co, Cr, Cu, Mn, Mo, Ni, Pb, Sb, Se, Tl, V, Zn, Th, and U)
- CLU2-2Y: Claritas Uranium Single Element Standard (1000 mg/L)
- CLHG2-1AY: Claritas Mercury Single Element Standard (10 mg/L)

Standards were diluted to $\mu\text{g}/\text{kg}$ concentrations appropriate for ICP–MS analysis in 5% nitric acid in deionized water solution to match the acid matrix of samples. Standards of 0.1, 0.4, 1.0, 4.0, and 10 $\mu\text{g}/\text{kg}$, were made up in 5% HNO_3 , and matrix matched for ICP–MS calibration.

Blank Preparations

Optima-grade nitric acid used in digestion was added to the deionized water blanks prior to analysis in a comparable concentration as to the

acid concentration found in the pet food samples. In addition to water blanks, optima-grade nitric acid was processed as a sample in the microwave vessel to determine contamination from the polytetrafluoroethylene (PTFE) vessels or any memory effects of the previous samples. After each pet food sample digestion run, 10 mL of nitric acid were digested discarded from the microwave vessels to clean vessels. A second 10 mL digestion of nitric acid was then repeated, and the digest was diluted in the same method as the pet food samples and treated as a vessel blank.

Sample Collection, Preparation, and Digestion

For this investigation, a total of 61 different cat and dog foods were bought from local stores or donated by employees of the SPEX companies and CEM Corporation. The samples consisted of dry food varieties. Of the 60 dry foods, 37 of them were dog food, and 23 of them were cat food samples. The range of quality of the pet foods was from "discount" to "gourmet brands." Pet food prices ranged from the "bargain" store foods priced at 0.02¢ per ounce to gourmet or specialty foods purchased from pet suppliers priced above 0.42¢ per ounce. There are 11 samples that were similar or identical to brands or varieties studied in the original 2009 study.

Dry cat and dog food samples (10–15 g) were ground to a uniform powder in a cryogenic mill (SPEX SamplePrep 6875D Large Dual Freezer/Mill with 6885 mid-size Poly-Vial). Operating conditions are shown in Table 1

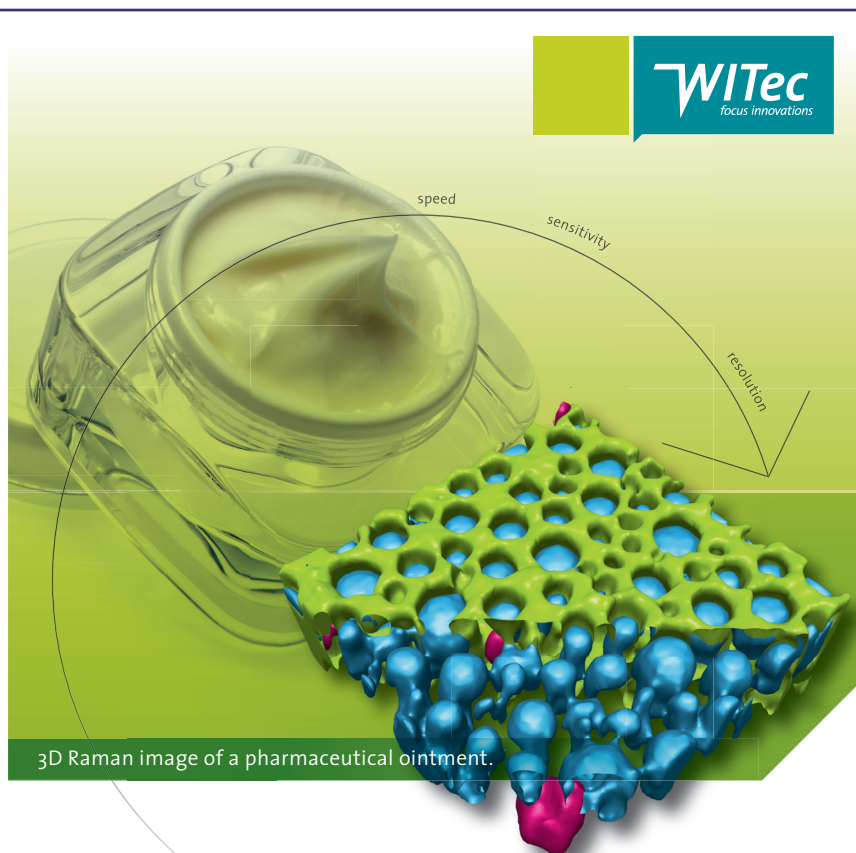
One half gram of the powdered or blended sample was digested with 10 ml of nitric acid in a CEM Mars-6 microwave oven (CEM Corporation) using a preprogrammed pet food method. After digestion, samples were diluted to 50 mL volume with deionized water. Prior to analysis, samples were diluted to a final concentration of 1000x using deionized water.

Instrument Conditions

Primary sample analysis was conducted using a PerkinElmer inductively coupled plasma–optical emission spectrometer (ICP–OES) (PerkinElmer Inc.). The ICP–OES was used to determine the macro-elemental composition of the foods to select standards which would allow for correct matrix interferences. Elements measured by ICP–OES included aluminum, calcium, copper,

iron, magnesium, manganese, phosphorus, potassium, selenium, silicon, sodium, sulfur, and zinc.

All trace element determinations were carried out using the Agilent 7900 ICP–MS (Agilent Technologies). It can be seen that multiple isotopes were used for many of the elements to evaluate the spectral complexity of the samples and also for mathematical equation correction purposes.



3D Raman image of a pharmaceutical ointment.

3D Raman Imaging

Turn ideas into **discoveries**



Let your discoveries lead the scientific future. Like no other system, WITec's confocal 3D Raman microscopes allow for cutting-edge chemical imaging and correlative microscopy with AFM, SNOM, SEM or Profilometry. Discuss your ideas with us at info@witec.de.

Raman · AFM · SNOM · RISE

www.witec.de

MADE IN GERMANY

Nanoscale IR Spectroscopy

Nanoscale infrared (nanoIR) spectroscopy has been commercialized for a little over 10 years. Since then, atomic force microscope infrared (AFM-IR) spectroscopy has seen a lot of growth, with dramatic changes in life science applications and nanoscale characterization of cells and tissues.

SPECTROSCOPY: It has been 10 years since the first nanoIR product was introduced. What are the main factors that led to the growth we've seen in the AFM-IR products Bruker manufactures?

MARCOTT: Originally, from the spectroscopist's point of view, the ability to obtain infrared spectra at spatial resolutions two orders of magnitude smaller than the diffraction limit was a tremendous breakthrough.

The spatial resolution of conventional Fourier-transform infrared (FTIR) microscopes is about 3 to 10 micrometers or roughly equal to the wavelength of light used to make the measurement. In AFM-IR, the sharp tip of the atomic force microscope acts as a local detector of IR absorbance at the surface of the sample it contacts. When the wavenumber of the laser source is in resonance with a molecular vibrational frequency, the IR radiation can be absorbed, and the sample expands when the molecules return to their ground vibrational state after exchanging energy with the sample matrix. This causes the sample to thermally expand over an area corresponding to the focused IR laser spot size. The AFM cantilever will deflect because the local thermal expansion of the material in proximity to the apex of the AFM probe is providing significantly higher spatial resolution that is not limited by the diffraction limit of the IR wavelength.

A key enabler for the emergence of the AFM-IR technique was the availability of reliable, broadly tunable IR laser sources. The ability to add nanoscale chemical information to high-resolution spatial topography maps opens up a whole new toolbox for developing nanomaterials and understanding their structure and properties.

Another key point is that the photothermal AFM-IR signal is directly proportional to the exact amount of IR radiation absorbed at a particular wavenumber. This means AFM-IR spectra have no band distortions due to scattering. Thus, photothermal AFM-IR spectra look identical to thin film FTIR spectra collected in transmission and can be digitally searched against commercial databases or user generated libraries of reference spectra.

SPECTROSCOPY: What are some of the key technological advances over the past 10 years that have led to the growth of AFM-IR technology?

MARCOTT: Many of the technological advances have been the result of improved laser sources. For example, the ability to match the



Dr. Curtis Marcott
Senior Partner
Light Light Solutions

Sponsored by



repetition rate of the pulsed tunable IR source to be in resonance with an AFM cantilever ringdown frequency improves the sensitivity of AFM-IR by two orders of magnitude.

Initially, AFM-IR measurements needed to be made in contact mode. Laser sources with faster repetition rates enable the measurements to be made in tapping mode, which is important because not all samples can be measured in contact mode. In addition, increased laser-tuning speed has enabled measurements to be performed much faster. Also, broader spectral tuning ranges that were not accessible 10 years ago are now available.

SPECTROSCOPY: Initially, most AFM-IR applications were directed toward chemical characterization of polymers and other materials. What about applications in the life sciences?

MARCOTT: It's taken longer for life-science applications of AFM-IR to take off, but that changed dramatically in the past few years with many exciting new developments. With traditional commercial FTIR microscopes, it was not possible to look at subcellular structures, as the typical size of a single cell is about the same size or even smaller than a single spatial resolution element. In biology, many important processes occur at the subcellular level. These can now be followed for the first time by AFM-IR.

SPECTROSCOPY: What are some examples of recent work in the area of nanoscale characterization of cells and tissue using AFM-IR?

MARCOTT: Protein misfolding is one area that is important to understand as it relates to the developments of fibrils found in diseases like Alzheimer's, Parkinson's, and Huntington's. With AFM-IR, it's possible to characterize the protein secondary structure of individual plaque fibrils and their precursors, which has provided insights into the mechanism of fibril formation.

It has recently been demonstrated that protein secondary structure can even be determined for a single protein molecule. Much of this pioneering work was done by Professor Francesco Simone Ruggeri, now at Wageningen University in the Netherlands.

There are many other examples of AFM-IR studies of cells and tissues. For example, in a recent paper from Monash University, AFM-IR probed the phenotype of the malaria parasite during its development. The ability to monitor in-vivo changes during cellular processes in bacteria at the nanoscale has also been demonstrated by the Monash group.

This opens up a new platform to study environmental influences and other factors that affect bacterial chemistry, including antimicrobial resistance detection at the single bacteria level. In a recent paper from the University of Sydney, AFM-IR provided unparalleled nanoscale characterization of the physical and chemical composition of individual liposomes encapsulating ciprofloxacin, including the successful differentiation of empty liposomes from liposomes encapsulating ciprofloxacin in dissolved and nanocrystalline form.

Another paper from the Polish Academy of Science showed the AFM-IR technique can be a powerful tool for tracking biomedical changes of marginal and neoplasm tissues, revealing crucial details about the mechanism of pathological state development not observable using conventional vibrational spectroscopic methods. These are just a few examples of exciting applications of AFM-IR to the characterization of cells and tissues.

SPECTROSCOPY: Much biological activity occurs in the presence of water. Are there recent advances that allow for AFM-IR measurements to be made in fluids?

MARCOTT: There's an excellent 2018 paper in *ACS Nano* in which the authors discuss a significant extension of nanoscale polypeptide conformational analysis to aqueous environments. Proteins are central to essentially all molecular processes and living organisms, typically carrying out their activities by folding to well-defined three-dimensional structures and by binding to other molecular species to form functional complexes. IR spectroscopy is well-established as an important measurement capability for chemically characterizing the secondary structure of proteins both in solution and in the solid state.

Differences in the Amide I band contour indicate the presence of different secondary structures in the protein. AFM-IR has been shown to be very sensitive to protein secondary structures at the nanoscale, but until recently, could only be performed on dried materials. There's always a concern that drying out the protein-containing material may result in a confirmation change in the protein backbone structure.

The new approach and results described in this *ACS Nano* paper show that it is now possible to generate nanoscale-resolved IR spectra and maps, in air and water with comparable spectral band contours, signal-to-noise ratio, and lateral spatial resolution.

TABLE V: Table of 2019 select toxic metal concentrations in 3 cups of dry dog food (in ug)

2019 Samples (µg/serving)	As	Be	Cd	Ni	Pb	Sb	U
Highest EPA RfD or WHO TDI	49	45	23	454	82	138	68
Dog-1	33	36	9	763	32	5	15
Dog-2	28	38	8	442	19	2	28
Dog-3	26	39	16	351	17	2	21
Dog-4	125	37	10	416	38	2	9
Dog-5	53	34	16	404	119	16	7
Dog-6	54	31	16	626	155	18	10
Dog-7	152	56	14	645	37	7	46
Dog-8	83	109	25	635	46	13	216
Dog-9	206	39	11	361	54	4	34
Dog-10	39	47	10	846	47	48	58
Dog-11	16	31	5	821	20	3	4
Dog-12	111	40	11	354	40	8	34
Dog-14	133	114	42	583	154	15	280
Dog-15	64	77	21	408	69	8	166
Dog-17	107	36	12	349	43	4	16
Dog-18	93	36	10	345	44	8	4
Dog-19	69	50	13	371	25	9	95
Dog-20	46	53	26	504	25	6	90
Dog-21	18	35	ND	339	14	3	33
Dog-22	54	48	11	446	41	4	103
Dog-23	104	65	21	390	34	8	456
Dog-24	73	66	16	556	55	8	192
Dog-25	54	48	12	369	45	5	236
Dog-26	124	54	16	319	33	7	322
Dog-27	168	72	15	309	37	9	510
Dog-28	49	43	14	405	73	5	9
Dog-29	56	33	18	402	72	4	7
Dog-30	33	41	25	590	80	5	5
Dog-31	21	35	40	632	20	3	4
Dog-32	70	32	27	474	23	1	5
Dog-33	57	37	14	609	52	96	4
Dog-34	64	30	11	499	38	2	8
Dog-35	100	41	17	812	76	5	19
Dog-36	58	42	22	1764	97	5	14
2019 Mean (µg/serving)	75	49	17	549	51	10	97
2019 Max (µg/serving)	206	114	42	1764	155	96	510

TABLE VI: Comparison of exposure of selected elements in 2009 and 2019 dog food samples

Element	EPA (RfD μg)	WHO (TDI μg)	2009 Mean (μg)	2019 Mean (μg)	2009 Max (μg)	2019 Max (μg)	2009 Mean % Limit	2019 Mean % Limit	2009 Max % Limit	2019 Max % Limit
As	7	49	41	75	74	206	84%	154%	152%	420%
Be	45	None	6	49	22	114	13%	109%	49%	253%
Cd	23	23	20	17	39	42	87%	74%	170%	183%
Ni	454	272	377	549	833	1764	83%	121%	183%	389%
Pb	None	82	59	51	280	155	72%	63%	341%	189%
Sb	9	138	46	10	289	96	34%	7%	210%	70%
U	68	14	70	97	259	510	103%	142%	381%	750%

Wherever possible, the most sensitive isotope free of spectral interferences was chosen for the quantitation.

Results and Discussion

Heavy Metal Concentrations 2009 and 2019

In 2009, there were significant amounts of metals found in the pet food, with 215 ppm aluminum and over 1 ppm of several potentially toxic metals, including chromium (2.5 ppm), nickel (3.2 ppm), lead (6 ppm), and tin (9.4 ppm). There was 0.5 to 1 ppm of antimony and cobalt. Some foods had correlations of ppm levels of nickel and tin showing large amounts of potential wear metal contamination from the manufacturing equipment. There was even uranium detected in several samples up to 1 ppm.

The samples from 2019 still showed heavy metal contamination, including twice the amount of uranium (1.7 ppm), and three times the amount of arsenic (0.7 ppm). Lead levels were significantly lower overall in the 2019 samples with a maximum of 0.5 ppm, as shown in Table II.

In 2009, one of the surprises resulting from the analysis was the discovery of up to 1 ppm of uranium in the pet food samples. Later, it was discovered there was a correlation of samples

containing uranium also having significant levels of beryllium and thorium, as shown in Figure 1.

In the 2019 study, the levels of uranium, beryllium, and thorium were again examined, and it was found that the 2019 samples had a greater number of samples that contained significant uranium levels than in 2009. The samples set for 2019 contained fourteen samples over 250 ppb compared to only six samples in 2009. Most of the 2019 samples were dry dog foods, which was also consistent with the 2009 study, but in the updated samples, there were two dry cat foods which also measured over 250 ppb, whereas in 2009 there were only dry dog food samples. Nine 2019 samples contained over 500 ppb and four had over 1 ppm, with the highest sample at 1.7 ppm of uranium.

Exposure and Daily Limits

In 2009, as was stated earlier, there were no limits or guidelines for heavy metals in pet food, so limits were used for human exposure from the U.S. Environmental Protection Agency (EPA) and World Health Organization (WHO). Average pet size was standardized to 50 lbs for a dog and 10 lbs for a cat. At the time of the 2009 study, a survey of feeding habits was

conducted amongst the owners of the donated pet food. Most owners in general fed their pet approximately one cup of food per 10 lbs of body weight per day. After the publication of the study, some parties (pet food companies) expressed concern and criticism for the amount of food being fed and therefore the potential elemental exposure. In light of these comments, in the 2019 study, veterinary guidelines for the feeding of pets limited the food consumption to approximately three cups of dry dog food and one-half cup of dry cat food daily.

During the interim between studies, the 2011 FSMA was implemented. In the act, there was further guidance on the safety of pet food, but, again, no limits were expressed for heavy metals or toxic elements in pet food so updated human limits from the WHO and the EPA were used as guidelines. Reference daily dosages (RfD) and tolerable daily intake (TDI) for the pets were calculated (Tables III and IV) to estimate exposure from the various foods tested.

Dog Food Exposure Results

The 2019 samples results were calculated for a serving of three cups of dry dog food intended for a 50-lb dog (Table V) and compared to calculated limits (Table III). Mercury results were

TABLE VII: Table of 2019 select toxic metal concentrations in 1 cup of cat dog food (μg per serving) and comparison to 2009 Results.

2019 Cat (μg /serving)	As	Cd	Ni	Pb	U
Max EPA RfD or WHO TDI	10	5	91	16	14
Cat-1	5	1	92	9	ND
Cat-2	35	2	120	12	0
Cat-3	40	4	91	12	1
Cat-4	6	5	110	2	1
Cat-5	7	ND	35	5	ND
Cat-6	11	5	80	17	25
Cat-7	5	3	50	8	16
Cat-8	13	6	60	13	29
Cat-9	2	2	81	14	0
Cat-10	6	3	71	12	16
Cat-11	10	1	99	18	ND
Cat-12	16	2	93	8	2
Cat-13	13	2	85	15	ND
Cat-14	4	2	119	5	5
Cat-15	24	2	102	10	0
Cat-16	8	2	109	7	8
Cat-17	2	1	94	4	0
Cat-18	6	1	123	6	1
Cat-19	26	1	119	12	1
Cat-20	29	2	99	12	0
Cat-21	9	0	52	3	0
Cat-22	27	1	134	10	5
Cat-23	6	2	174	13	0
2019 Mean (μg)	14	2	112	11	5
2019 Max (μg)	40	6	399	43	29
2019 Mean % Limit	140%	40%	123%	69%	36%
2019 Max % Limit	404%	120%	438%	269%	207%
2009 Mean (μg)	9	3	94	39	2
2009 Max (μg)	18	4	191	355	14
2009 Mean % Limit	94%	51%	104%	243%	17%
2009 Max % Limit	176%	84%	210%	2216%	97%

not included in 2019 data because of technical issues.

The exposure for many of the elements increased from 2009 to 2019

as well as the proportion of samples with high levels of metals. In 2009, arsenic was high for 44% of dog food samples, but in 2019, 70% of samples

exceeded the highest WHO daily limit for 50 lbs of body weight. Nickel exposure overages also increased from 22%, exceeding limits in 2009 to al-

most 46% over in 2019. Some exposures for lead and cadmium dropped from 2009 to 2019. Lead dropped from 22% over limit in 2009 to 11% over in 2019. Cadmium dropped from 28 to 19% over RfD.

The concentration of heavy or toxic metals in the food increased for most elements, with higher mean and maximum results in 2019 compared to the results from 2009 (Table V). In both studies, the maximum measured elemental content approached or exceeded allowable daily limits of exposure. In 2009, arsenic concentration was 84 (mean) to 152% of the limit, but in 2019, arsenic ranged from 153 (mean) to 420% (maximum) of the highest WHO limit, as seen in Table VI.

Cat Food Exposure Results

Cat food, similar to dog food, found increases in concentrations of trace elements from 2009 to 2019. The total number of samples with levels that exceeded limits increased as did the overall concentrations of elements, such as arsenic, nickel, and uranium. The majority of cat food samples had arsenic levels above the WHO TDI. The highest samples contained over 400% the limit. As was found in the dog food, lead levels were slightly lower in the 2019 samples compared to the 2009 data, as seen in Tables VII.

Conclusions

The quality control procedures used in the past to produce cat and dog food were not equal to foods for human consumption as was shown in the 2009 study. This fact was particularly apparent in dry cat and dog food formulas, which might contain up to a dozen different ingredients, such as animal parts, meat byproducts, cereals, fillers, nutrients, and essential minerals.

The enactment of the FSMA did include pet food in the scope of food safety, but still there are no definitive limits for heavy and toxic metals for pet food which can either be derived from raw materials (such as fillers, grains, cereals, or meals) or processing equipment. Essential minerals like calcium and phos-

phorus are manufactured from industrial chemicals, which could possibly contain other trace metal impurities. The purpose of the original study and the updated 2019 study was not to track down the source of the elements and contamination found in pet food, but an attempt to evaluate significant levels of metals in the food.

The interest in this study and its predecessor becomes relevant when the data is compared to the EPA RfD and WHO TDI values. These are guidelines that are set down by experts in the scientific, medical, and health care communities, based on decades of research into toxicity. In lieu of validated limits for dogs and cats, we choose to be cautious and use the human limits to compare exposure levels potentially found in an animal's daily consumption of dry pet food.

The metal content of many of the different pet foods is significantly higher than EPA and WHO values, when adjusted for the average weight of a dog and cat. We do not know the chemical composition or speciation of the heavy metals found in these foods, and therefore, we do not know their uptake or bioavailability, and we also do not know if the EPA RfD and WHO TDI values apply the same to animal physiology.

The 10 years between the two pet food studies did not show any major drops in heavy metal contamination despite the enactment of the FSMA. Some of the lead levels have dropped but other potentially toxic metals have increased, including arsenic, nickel, and uranium. The 2019 samples showed uranium in cat food unlike the 2009 study which only found uranium in the dog foods. There are many studies regarding heavy metals and toxic metals in human foods which go undetected, so it is not surprising that pet food is still not comprehensively tested for metals contamination.

Acknowledgments

The updated 2019 study is a joint effort between the scientific teams and employees of SPEX CertiPrep,

SPEX SamplePrep, and CEM Corporation. Special acknowledgement for the sample grinding conducted by Eric Smith of SPEX SamplePrep and sample preparation and digestion by the team at CEM, including Tina Restivo, Bob Lockerman, and Macy Harris. I would also like to acknowledge the SPEX CertiPrep inorganic analytical team, including William Green, Katherine Cullen, and Alan H. Katz, as well as many other assistants, chemists, and technicians in the SPEX Inorganics department, without whom the data would never have been processed.

References

- (1) P. Atkins, L. Ernyei, W. Driscoll, R. Obenauf, and R. Thomas, *Spectroscopy* **26**(1), 46–56 (2011).
- (2) P. Atkins, L. Ernyei, W. Driscoll, R. Obenauf, and R. Thomas, *Spectroscopy* **26**(2), 42–59 (2011).
- (3) L. Bush, *Spectroscopy* **35**(12), 22 (2020).

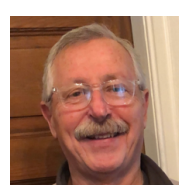
ABOUT THE AUTHORS



Patti Atkins is a Senior Applications Scientist at SPEX CertiPrep and a member many scientific committees, including NACRW, AOAC and ASTM.

Tina Restivo is a Senior Scientist at CEM Corp. **Bob Lockerman** is the Global Analytical Product Manager for the MARS 6 microwave digestion system at CEM Corp. Direct correspondence to: patkins@spex.com •

ABOUT THE COLUMN EDITOR



Robert Thomas is the principal of Scientific Solutions, an educational consulting company that serves the training and writing needs of the trace element user community. He has worked in the field of atomic and mass spectroscopy for more than 45 years. •

Library Searching

Brian C. Smith

One of the biggest practical limitations of infrared spectroscopy is its difficulty in analyzing mixtures. The root cause of the problem is that the more different types of molecules there are in a sample, the more difficult it becomes to figure out which peaks are from which molecules.

In a previous column, we discussed a number of techniques to make the mixture analysis problem easier, including purification, spectral subtraction, and library searching (1). At that time, I promised to write a future column with more details on library searching and spectral subtraction. A search of my records shows that I never wrote that column, and I apologize for that. This column, therefore, focuses on library searching, and a future column will focus on spectral subtraction.

Spectral Comparisons

Spectral comparisons, where a known reference spectrum is compared to an unknown spectrum to assist in its identification, is an important tool in infrared spectral interpretation (2). I am old enough that I began interpreting spectra before personal computers were invented. Back in those Jurassic days, to identify an unknown one had to compare the sample spectrum to paper copies of known spectra kept in hundreds of green three-ring binders. It could take hours of poring over these dusty tomes to find the correct library match. The company back then that published these spectra was called Sadtler Chemical (3).

Fortunately, computerized library searching now exists. In this technique, an unknown spectrum is compared to a collection of known infrared spectra kept in a digital infrared spectral library. Revealing my age once again, the first Fourier transform infrared (FT-IR) system I ever used that had computerized library searching capabilities took 15 min to complete one

library search! I should point out that this system had a computer, manufactured by the FT-IR maker, with a whopping 64 kb of memory. Here in 2021, I think my toaster has more computing capability than my FT-IR computer did back then. Today, of course, library searches of thousands of spectra take place in a flash.

Regardless of the computer, a library search is performed by mathematically comparing your unknown spectrum to each of the spectra in a library. If there are 1000 spectra in the library, then 1000 comparisons will be performed. The library search software uses what is called a search algorithm to generate a number describing how similar, or different, the two spectra are. This number is called a Hit Quality Index (or HQI, for short), and it is discussed later on in the column.

Where Can I Buy Infrared Spectral Libraries?

To perform library searching, the first thing you have to do is obtain some libraries. I normally don't call out individual companies in this column, but there are only a handful of companies selling infrared spectral libraries, so I will name several here as a convenience to my readers. I apologize if I leave anyone out.

The company with perhaps the largest collection of infrared spectral libraries is what was Sadtler, became Bio-Rad, and is now part of Wiley (3–5). According to their website, Wiley has available 264,000 spectra you can search against (5). Access to these libraries is normally done via a leasing arrangement.

Another vendor that sells infrared spectral libraries is Sigma-Aldrich (6). As far as I can tell, their entire collection consists of about 100,000 spectra. A couple of smaller companies that sell infrared spectral libraries include ST Japan (7) and Fiveash Data Management (8). A Google search will also turn up some free libraries on the internet. My experience with free libraries is that they are generally small and specific to a narrow range of samples, and sometimes the data are not correct because they have not been vetted properly. As a result, be very careful when using free libraries off the internet. The libraries you purchase may come on a compact disk, be copied to your computer's storage device, or installed on your company's computer network.

Ultimately, the best source of infrared spectral libraries is you. Most FT-IR software packages allow you to build your own libraries. I strongly encourage this, because only you have access to the

sample types typical of your work. You can even build multiple libraries of your own of different types. For example, you could build your own polymer, gas phase, and inorganics library, and search appropriate unknowns against them. Every time you come across a new sample for which you have a good identification, add it to an appropriate library. Spectra you add to your libraries become de facto references. For this reason, please make sure your data is of high quality, you are certain of the identification, and the data matches the instrumental resolution of the other spectra in the library (9).

What About the Instrumental Resolution of Library Spectra?

Instrumental resolution is a measure of how well a spectrometer distinguishes spectral features from each other (9). In FT-IR, instrumental resolution is measured in cm^{-1} . For example, a spectrum measured at 8 cm^{-1} resolution can resolve

features that are 8 cm^{-1} or further apart (9). When library searching is performed, the unknown and library spectra must be measured at the same instrumental resolution. This is why when you purchase infrared spectral libraries, they come in different resolutions. For example, the same library might be available in 8 cm^{-1} and 4 cm^{-1} resolutions. When purchasing a library, you must make sure that the libraries' resolution matches that of the samples you will be measuring.

The Search Process

What Libraries Should I Use?

After starting up your library searching software package, you will need to choose which libraries to search against. It may be tempting to try the shotgun approach and search your sample spectrum against all the libraries you have, but this may end up being a waste of time. Think about the nature of your sample. For example, a spectrum of a polymer searched against

We're Sensitive to Raman

We know it needs to be sensitive, robust, and reproducible, with components that adapt to **your** unique needs. From research in the lab to product design for the field, our toolbox gives you superior sensitivity & speed in a choice of flexible, compact footprints, 248 to 1064 nm.

FLEXIBLE & MODULAR

spectrometers mate easily to a probe or custom optics. Streamline your design with our new onboard laser models and automated operation!



COMPACT & INTEGRATED

systems incorporate a laser and sampling optics for maximum sensitivity and durability in the smallest footprint.

USER-CONFIGURABLE RAMAN PROBES

featuring a unique interchangeable barrel design, customizable to your application needs. Choose from standard options for lab and process or our new optical adapter kit.

SOFTWARE, SDKS & LIBRARIES

with the flexibility to capture, control, and analyze spectra on your own terms.

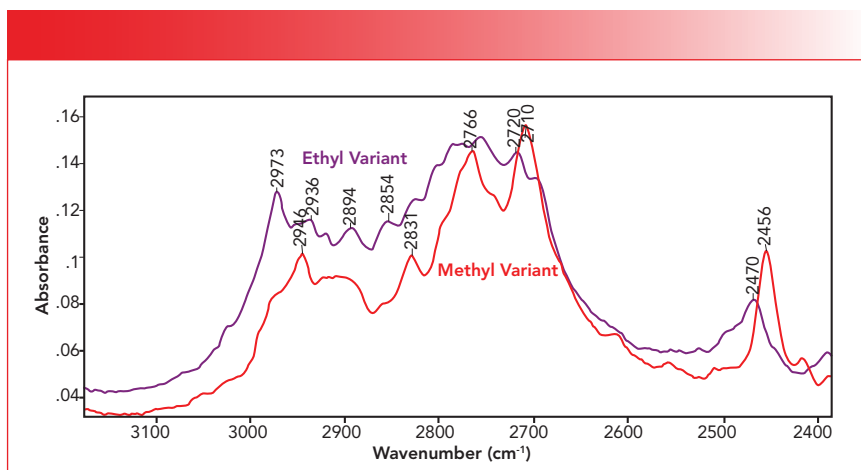


FIGURE 1: A comparison of the C-H stretching region of the methyl and ethyl variants of a controlled substance. Note the differences between the spectra.

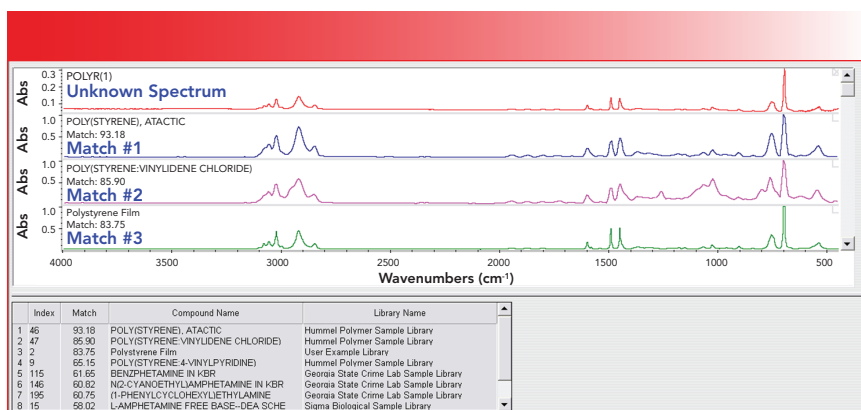


FIGURE 2: An example of a search report. The sample spectrum was of pure polystyrene, and the correlation search algorithm was used.

a gas phase spectral library will never produce good results. On the other hand, a polymer spectrum searched against a large organics library might yield good results if the repeat unit of the polymer is similar to any of the molecules in the library. Judicious choice then of what libraries you search against is important.

What Wavenumber Regions Should I Use?

Another thing to think about before performing a library search is to select what wavenumber region or regions to use. Typically, the default region in use by your search software will be the entire spectrum, let's say 4000 to 400 cm^{-1} . However, the software will typically allow you to choose spectral regions to include or exclude from the search, and this some-

times makes sense. For example, if your sample spectrum has unwanted water vapor or CO_2 peaks, you should exclude those regions from your search, since they are not part of the sample and their presence can throw off your search results. Additionally, if a sample is a mixture and you have identified a major component, excluding its peaks from a search might make the search more sensitive to the identity of minor components.

Some years ago, while I was consulting for a forensics laboratory, they had a problem distinguishing between the methyl (CH_3 -) and ethyl (CH_3 - CH_2 -) variants of a controlled substance using library searching. They were using the sample's full spectrum in the search. Considering the chemical differences between the two variants, I thought it made sense to look

at the C-H stretching region, which is from 3200 to 2800 cm^{-1} as we have discussed in previous columns (2). A comparison of the spectra of the two variants in this region is seen in Figure 1.

Note that the spectra are similar but not identical. By narrowing the wavenumber region used in the search to that seen in Figure 1, a library search was then able to distinguish between these two variants and the problem was solved. This a real and powerful example of how judiciously choosing the spectral regions used in a search can improve search results.

What Search Algorithm Should I Use?

A search algorithm is the mathematical calculation used to compare two spectra to each other and generate a HQI. A discussion of these algorithms is beyond the scope of this article, but you can find more info in the help function of your library search software or here (9).

Most library searching software packages present you with a choice of search algorithms. The differences between these algorithms is that some emphasize peak position, some emphasize peak height, and some strike a balance between the two. Algorithms with the word "derivative" in them tend to emphasize peak positions, algorithms with the words "absolute" or "absolute value" tend to emphasize peak heights, and two algorithms that strike a balance are euclidean distance and correlation (9).

From my own experience, I find that balanced algorithms, such as correlation and euclidean distance, are good for general search purposes. However, if a given search algorithm does not produce satisfactory results, it is all right to change the search algorithm and see if it improves your results. It is generally easy to switch search algorithms in library search software packages, so this is a parameter you can experiment with.

The Search Report

Recall that the number of spectral comparisons performed equals the number of spectra in your library. Manually sorting through all these matches would be a challenge, but fortunately the search software

program organizes the hits and presents the best ones in the form of a search report. An example of a search report is seen in Figure 2. The “unknown” spectrum was of pure polystyrene, and the correlation search algorithm was used.

The table at the bottom of Figure 2 lists the identity of the eight best hits along with the HQIs and the library where the example spectrum was found. In the software used in this example, a 0 to 100 HQI scale was used, where 100 is a perfect match, and 0 is the worst possible match. Also note that the search report shows the sample spectrum and the spectra of the best matches. The best match, with an HQI of 93.18, is of pure polystyrene, which is good and expected. The second best match, with an HQI of 85.90, is of a mixture of polystyrene and another polymer. This makes sense, since impure polystyrene should be a worse match than pure polystyrene.

Making Sense of the HQI

HQIs are useful indicators of spectral similarity, but they are not perfect. Random similarity in the noise and artifacts between two spectra can give search results more similar than reality. Conversely, random differences in noise and artifacts between two spectra can make them poorer matches than reality. This is why the HQI by itself should never be used to identify a sample. I have seen inexperienced people look at a search report, incorrectly assume the first match in the table identifies the sample, and suffer career-ending consequences.

Search algorithms are just mathematical formulas; they do not understand spectroscopy or chemistry and make mistakes. I cannot emphasize enough the importance of always visually comparing the sample spectrum to that of the best library matches. The HQI is not a measure of the probability of having found the right answer; it is not a measure of purity. It is strictly used to organize the matches for a given search. The search will always produce a result whether there are any good matches or not, and the fact that there is a result does not mean you have identified the sample.

Ultimately, it is your job as the user of the search software, and not the computer’s (since you have a brain and eyeballs), to make the final conclusion as to the identity of a sample based on a library search. The library search narrows things down for you; it is your job to make the final decision as to whether two spectra are a match or not.

How then do we interpret the HQI? At minimum, the range of the HQI can be useful. Assuming a 0 to 100 HQI scale as discussed above, matches between 80 and 100 are excellent and may be good enough to obtain an identification. HQIs between 50 and 80 are good, but typically not good enough for a complete identification. However, you can often times obtain information about the functional groups present from matches of this quality. Lastly, a HQI less than 50 is a poor result, and is generally not useful.

What Do I Do About Poor Search Results?

You could panic, but that is not an appropriate response for a scientist, unless said scientist is being chased by a grizzly bear (more on that in a later column). Ultimately, bad library search results are not necessarily your fault—you are at the mercy of the libraries you have access to. If, by chance, your unknown looks nothing like any of the spectra in your libraries, there is not much to be done about it. This is an argument then for having access to a large number of library spectra so you can maximize the probability of finding a good match. Additionally, remember that you can experiment with wavenumber regions and search algorithms to try and improve your search results.

Conclusions

Infrared spectral library searching is useful in identifying unknowns and in mixture analysis. It works by mathematically comparing your sample spectrum to a collection of spectra kept in a digital library. HQI measures how similar or different two spectra are. However, the HQI only ranks the quality of the matches for a given search, and should not be used by itself to

make an identification. Visual comparison of the sample and library spectra should be used in combination with the HQI to achieve a sample identification. Experimenting with the search algorithm and wavenumber region may improve search results.

References

- (1) B. C. Smith, *Spectroscopy* **30**(7), 26–31, 48 (2015).
- (2) B. C. Smith, *Spectroscopy* **30**(9), 40–46, (2015).
- (3) www.sadtler.com.
- (4) Wiley Acquires Bio-Rad’s Informatics Spectroscopy Software and Spectral Databases | Business Wire
- (5) KnowItAll IR Spectral Database Collection - Wiley Science Solutions
- (6) FT-IR Spectral Libraries Nicolet/Aldrich Condensed Phase Library, edition 2 | Sigma-Aldrich
- (7) *Spectra Databases - katja-hm* (jimdo.free.com).
- (8) *FDM FTIR and Raman Libraries* (www.fdm-spectra.com).
- (9) B.C. Smith, *Fundamentals of Fourier Transform Infrared Spectroscopy 2nd Edition* (CRC Press, Boca Raton, 2011).



Brian C. Smith, PhD, is the founder and CEO of Big Sur Scientific, a maker of portable mid-infrared cannabis analyzers. He has over 30 years experience as an industrial infrared spectroscopist, has published numerous peer-reviewed papers, and has written three books on spectroscopy. As a trainer, he has helped thousands of people around the world improve their infrared analyses. In addition to writing for *Spectroscopy*, Dr. Smith writes a regular column for its sister publication *Cannabis Science and Technology* and sits on its editorial board. He earned his PhD in physical chemistry from Dartmouth College. He can be reached at: SpectroscopyEdit@MMHGroup.com ●

Analysis of a Mixture Solution Using Silver Nanoparticles Based on Surface-Enhanced Raman Spectroscopy (SERS)

Lin Bao, Siqingaowa Han, and Wuliji Hasi

Scopolamine and promethazine can be used as a substitute for heroin. It is relatively fast and simple to use surface-enhanced Raman spectroscopy (SERS) for the detection and monitoring of drug usage. Silver nanosol is an enhanced substrate that is commonly used in the SERS technique; the Raman signal of the sample is amplified by the substrate. However, for the detection of mixtures, the competitive adsorption of different components relative to the substrate will result in difficult qualitative identification of spectra. By taking advantage of this defect, the adsorbed components of a mixture were separated from silver nanoparticles by centrifugation, thus changing the mixing ratio of the two components in the mixture. As a result, the proportion of the components with strong adsorption in the mixture is relatively reduced. Thus, the components with weak adsorption can be displayed in the spectrum of the mixed solution.

Heroin is one of the most widely used narcotics in the world, and it is a key target to be monitored because of its addictive quality and the difficulty in quitting the addiction (1–6). After long-term use, heroin will cause serious damage to the nervous system of the human body, and will also adversely affect judgment, possibly causing harm to the addict or society (4,7,8). Some drug rehabilitation institutions use less harmful drug-like substances as substitutes to reduce the suffering of drug addicts and damage to their nervous system (9–14). For example, a mixture of buprenorphine, scopolamine, and promethazine, referred to as BSP, has been used because its toxicity is much lower than that of heroin (15). However, long-term use of BSP will still cause great damage to the human body (9,10). Because the price of BSP is low and it is easily accessible, it has become an alternative drug for some drug users. Therefore, it is necessary to engage in the detection and monitoring of this new type of drug abuse.

Surface-enhanced Raman spectroscopy (SERS) is a combination of Raman spectroscopy and nanotechnology, and it can enhance the Raman signal by 7–10 or-

ders of magnitude when the tested sample is near or adsorbed on a substrate at the nanometer scale (16–19). The Raman spectrum of each sample is specific, and can be qualitatively identified as the fingerprint of the sample.

There are two popular viewpoints about the enhancement mechanism of SERS: One viewpoint is electromagnetic enhancement, and the other viewpoint is chemical enhancement (17,20). Electromagnetic enhancement generally refers to the enhancement of Raman signals by the strong electromagnetic field generated by the local surface plasmon (LSPR) excited by the rough surface of metal materials or the surface of metal nanoparticles (21). The chemical mechanism refers to the contribution of Raman scattering independent of the electromagnetic environment (such as plasma polaritons). The increase in SERS signal is usually attributed to electron transfer between the adsorbed molecule and the substrate. Current research results show that the two enhancement mechanisms generally play a role at the same time, and that signal amplification effect of electromagnetic enhancement is greater than that of chemical enhancement. Based on these

enhancement phenomena, the SERS signal can be improved to some extent through substrate design or gap control (22–25).

Surface-enhanced spectroscopy as a drug detection technology has become increasingly mature (26–29). Because of its characteristics, it is more suitable for the detection of drugs in solution than many other analytical techniques. Compared with other detection technologies, the advantages of SERS lie in the simple operation of the instrument, the uncomplicated pretreatment of the sample before detection, the fast detection time, and the convenience of the portable instrument for the in situ detection of samples (30).

For SERS detection of mixtures, there are two problems associated with direct detection: One is the overlapping of peaks, and the other is competitive adsorption (31). Overlap of spectral peaks is most likely to occur when the molecular configurations of the components of the mixture are relatively similar.

There are some differences in the molecular configuration of the two components we tested. They were distinguished from the spectrum of the mixture as described in our previous studies (15). From the spectral observation, there is no chemical reaction of the two components after mixing; that is, no new substance is formed. The current study focuses on eliminating the interference of competitive adsorption in practical detection.

Experimental

Apparatus

A BWS415-785H portable Raman spectrometer (B&W Tek, Inc.) was used to obtain the spectral data. The maximum working power of the Raman spectrometer was 0.3 W. The laser wavelength was 785 nm. After spectrum acquisition, the spectrum is smoothed and the baseline was corrected by the instrument software.

The morphology of nanoparticles was characterized by a high-resolution field emission scanning electron microscope (Hitachi Company). The dynamic light scattering test was measured by a PALS/90P particle size analyzer (Brookhaven Instruments Co., Ltd.). A Cary 4000 UV-vis spectrophotometer was also used (Agilent Technology Co., Ltd.).

Reagents

Potassium iodide (KI), silver nitrate (AgNO_3), sodium citrate ($\text{C}_7\text{H}_5\text{Na}_3\text{O}_7$), and ascorbic acid ($\text{C}_6\text{H}_8\text{O}_6$) were purchased from Sinopharm Chemical Reagent Co., Ltd. Scopolamine hydrobromide powder (1G) and promethazine hydrochloride powder (5G) were purchased from Dalian Meilun Biotechnology Co., Ltd.

Sample and Substrates Preparation

The solutions of scopolamine and promethazine were obtained by diluting scopolamine hydrobromide and promethazine hydrochloride, respectively, with deionized water, are used to obtain solutions with different concentrations. Each solution is mixed with the substrate at the same time.

The preparation of the silver nano-substrate is as follows: Soluble silver salt nitrate (AgNO_3) was used as an oxidant, and

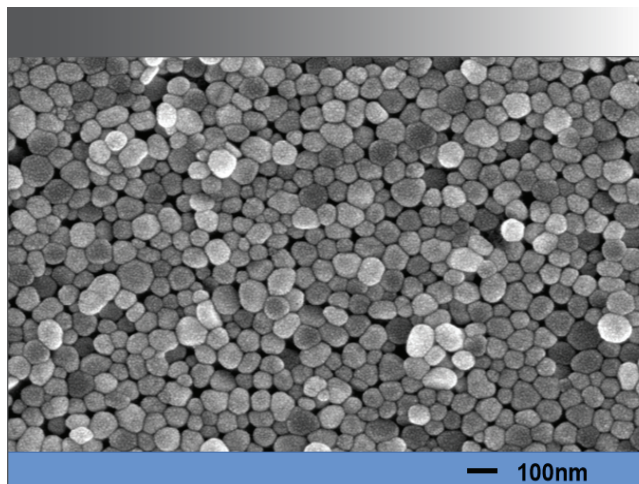


FIGURE 1: SEM image of silver sol substrate.

ascorbic acid was used as the reducing agent to prevent the aggregation of silver nanoparticles. Sodium citrate was used as the stable solution. Their concentrations in the initial solution were 0.168 mg/mL, 0.105 mg/mL, and 0.873 mg/mL. First, the water bath condition was prepared at 30 °C. Then, the three concentrations (soluble silver salt nitrate, ascorbic acid, and sodium citrate)

REFLEX ANALYTICAL CORPORATION

Serving you across the Spectrum

SPECTROSCOPY SUPPLIES AND ACCESSORIES

ONLINE ORDERING
PRODUCT SPECIALIST LIVE CHAT

★★★★★

CUVETTES
GAS CELLS
POLARIZERS
UHV VIEWPORTS
TUNGSTEN LAMPS
DEUTERIUM LAMPS
AA GRAPHITE TUBES
UV-VIS-NIR-IR CELLS
HOLLOW CATHODE LAMPS
BEAMSPLITTERS-FILTERS-LENSES
FTIR REFLECTANCE ACCESSORIES
ATR HEMISPHERES-PRISMS-RODS
HIGH PRESSURE TEMPERATURE CELLS
ICP GLASSWARE CONES COILS MULTIPLIERS
OPTICAL COATINGS METALLIZATION
VARIABLE PATHLENGTH GAS CELLS
XRF SOLID SAMPLING EQUIPMENT
VARIABLE TEMPERATURE CELLS
ONLINE PROCESS FLOW CELLS
XRF EVACUABLE PELLET DIES
LIQUID-SOLID-GAS CELLS
CRYOGENIC ACCESSORIES
GC CAPILLARY COLUMNS
LABORATORY PRESSES
GRINDING MILLS
PELLET DIES
OPTICS

WWW.REFLEXUSA.COM
201.444.8958 REFLEXUSA@ATT.NET



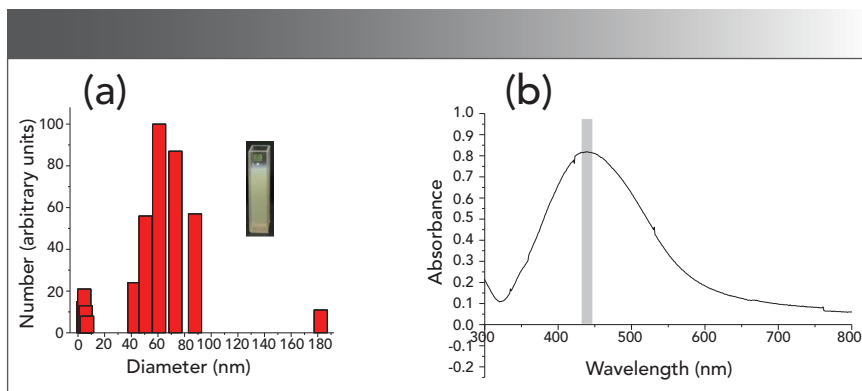


FIGURE 2: (a) Particle size distribution of silver sol; (b) UV-vis extinction spectra of silver sol.

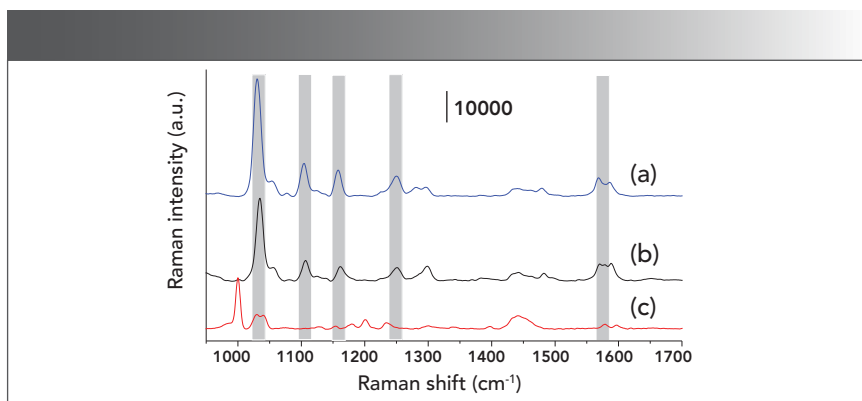


FIGURE 3: SERS spectra of (a) promethazine 10 ppm (3.5×10^{-5} M); (b) mixture at concentration ratio of 1:1 (1.5×10^{-5} M); (c) scopolamine 6 ppm (2×10^{-5} M).

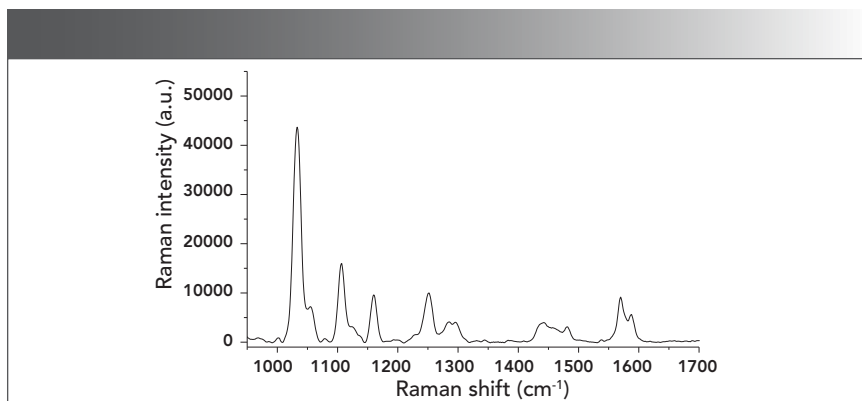


FIGURE 4: SERS spectra of mixture at concentration ratio of 1:1 (1.5×10^{-5} M) with potassium iodide (KI).

were placed in the bath proportional to each other, then the solutions (sols) were stirred continuously for 15 min with a magnetic mixture and both sol and nanosol are used. Then, the temperature of the water bath was continually raised to the boiling state and stayed at that temperature level for 2 h until the color

turned grayish-green. Then, the sol was refrigerated after cooling. Before using it, the sol needed to be centrifuged and purified to remove the smaller particles and improve the monodispersibility of the particles. Ultrasonic oscillation dispersion was performed before the test was used.

Results and Discussion

Figure 1 shows the SEM characterization of the silver sol substrate. The main process used is described in the literature (32). The silver nanoparticles are basically in a spherical state, and there is no mixing of other shapes of the substrate. Figure 2a shows the UV absorption spectrum, and the scanning range is from 300 nm to 800 nm. The absorption resonance peak is approximately 439 nm, which is consistent with the absorption peak of the silver sol. Figure 2b shows the statistical weight distribution of the particle size of the silver sol measured by dynamic light scattering (DLS) technology. Among them, 60 nm particles account for the largest proportion in the system, with its statistical weight being the total number of particles set to 100% and the statistical weight of other particle sizes compared with its value as the ordinate value of other particle sizes. It can be seen that several main particle sizes are distributed at 50–80 nm.

The SERS spectra of 10 ppm (3.5×10^{-5} M) promethazine and 6 ppm (2×10^{-5} M) scopolamine were used to compare the mixture, as shown in Figures 3a and 3c. It should be noted that because the signal of scopolamine is weak, the intensity of scopolamine is exaggerated by about three times. When the molar concentration ratio of the two mixtures was 1:1 (1.5×10^{-5} M), a weak Raman signal of scopolamine was detected at 1002 cm⁻¹. As shown in Figure 3b, the characteristic peaks in the mixture mainly belong to promethazine. However, in the previous study, when the concentration of the two components was the same, the spectrum was mainly the spectrum of scopolamine (15). The difference is that in our current study, the mixture was in contact with the silver nanoparticles at the same time; in the previous study, scopolamine was first added to the silver nanosol (nanosolution), and then the promethazine was subsequently added. From the trend of these two spectra, we can deduce that there is a competitive adsorption phenomenon when they are mixed simultaneously. Promethazine will mask the characteristic peak of scopolamine at the same concentration, which is not conducive to identify-

ing the spectrum of the mixture. What is more troublesome is that in the actual mixing ratio, the concentration of scopolamine is much lower than that of promethazine. To enhance the signal of scopolamine, we added potassium iodide into the mixture system to increase the strength of scopolamine.

To improve the signal of scopolamine in the mixed solution in Figure 3, we added potassium iodide (1 M). As shown in Figure 4, the signal of scopolamine at 1002 cm^{-1} increases with the addition of electrolytes, but it greatly decreases compared with the detection of scopolamine at the same concentration alone. Moreover, the concentration ratio of the silver sol we used is further increased, and the signal should be stronger in theory than what is shown in Figure 4. The characteristic peaks of promethazine in the spectrum of the mixed solution are basically all displayed. Promethazine of the same concentration was added to the electrolytes for independent detection and is compared with the mixture spectrum, as shown in Figure 5. The position and intensity of the peak of the mixture spectrum are almost the same as that of promethazine alone. Table I compares the intensity of the mixture spectrum with that of promethazine when it is separately detected in several main characteristic peaks. The results show that the signal of promethazine was dominant even though both of them were enhanced. This further shows that the enhanced signal of the two is mainly caused by the molecules adsorbing on the silver nanoparticles. The addition of electrolytes did not change the adsorption ratio of the two but further reduced the distance between nanoparticles and enhanced their signal.

In the mixture with the same concentration, the signal of scopolamine is weak, which is not conducive to spectral recognition. The more difficult problem is that the concentration of promethazine with strong adsorption is much higher than that of scopolamine in the actual ratio. It can predict the difficulty of actual detection. To verify this assumption, we mixed them according to the actual ratio, in which the mass concentration of scopolamine is 10 ppm ($3.3 \times 10^{-5}\text{ M}$), and the doping of promethazine is 1670 ppm ($5.9 \times 10^{-3}\text{ M}$). Through SERS detection, as shown in Figure 6a, scopolamine in the actual ratio cannot be identified in the Raman spectrum. Only the characteristic peaks of promethazine can be identified, which is consistent with the expected results.

According to the experimental verification, the nanoparticles in the silver sol are relatively easy to separate from the solution, as shown in Figure 8. For example, most of the nanoparticles will be located at the bottom of the tube after high-speed centrifugation. Figure 8a shows the original sol solution, and the supernatant after centrifugation is shown in Figure 8b. We used this method in combination with the "defects" of competitive adsorption to separate the components of the mixture in solution. After the mixed solution was added to the silver sol and then centrifuged, the silver sol traveled to the bottom of the centrifuge tube. Some samples adsorbed on the silver nanoparticles were separated from the mixed solution.

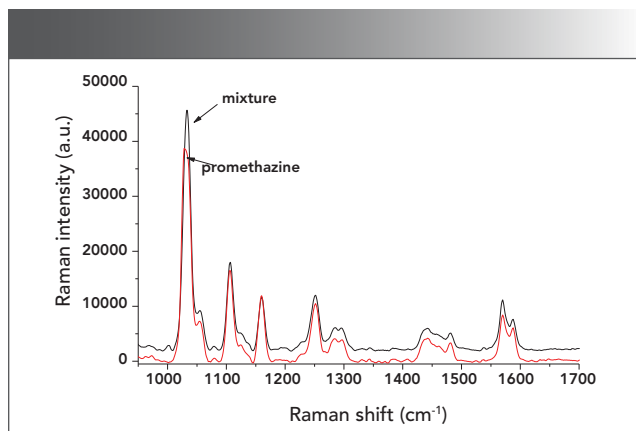


FIGURE 5: Comparison of SERS spectra between mixture and promethazine.

The adsorption of promethazine is stronger than that of scopolamine. Thus, promethazine should be the main component separated. The proportion of mixture in the remaining supernatant changed: The proportion of promethazine decreased, and the relative concentration of scopolamine increased. After repeating this several times, the characteristic peak of scopolamine can be seen in the mixed solution.

Are you compliant with the new European Pharmacopoeia 10.0 and USP <857> Standards?

Starna Certified Reference Materials provide an essential tool to achieving data integrity and compliance!



Wavelength accuracy: Deep UV to NIR
Absorbance accuracy & Photometric
Linearity: up to 3.5 A
Stray Light
Instrument Resolution
UKAS Accreditation as a:
Reference Material Producer -
ISO 17034
Calibration Laboratory -
ISO/IEC 17025
NIST Traceable
Lifetime Guarantee
Fast re-calibration service



Starna

Starna Scientific Ltd

Starna Cells Inc.
(800) 228-4482

sales@starnacells.com
www.starna.com

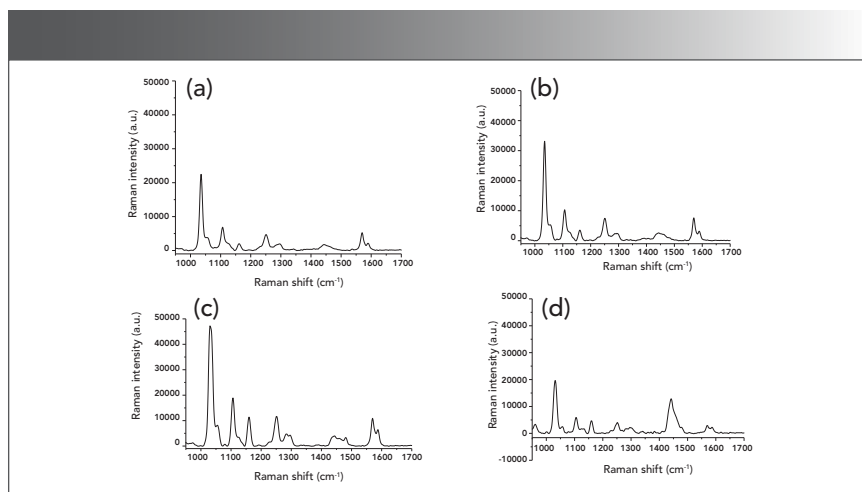


FIGURE 6: SERS spectra of mixture (a) original solution (promethazine: 5.9×10^{-3} M; scopolamine: 3.3×10^{-5} M) (b) the first centrifugation, (c) the second centrifugation, and (d) the last centrifugation.

TABLE I: Comparison of the main characteristic peaks of the two spectra

Raman Shift (cm ⁻¹)	Mixture Intensity (AU)	Promethazine Intensity (AU)	RSD (%)
1034	43228.32	37251.13	10.50
1105	15536.29	16314.15	3.45
1250	9833.036	10170.52	2.39
1569	9159.041	8409.041	6.04

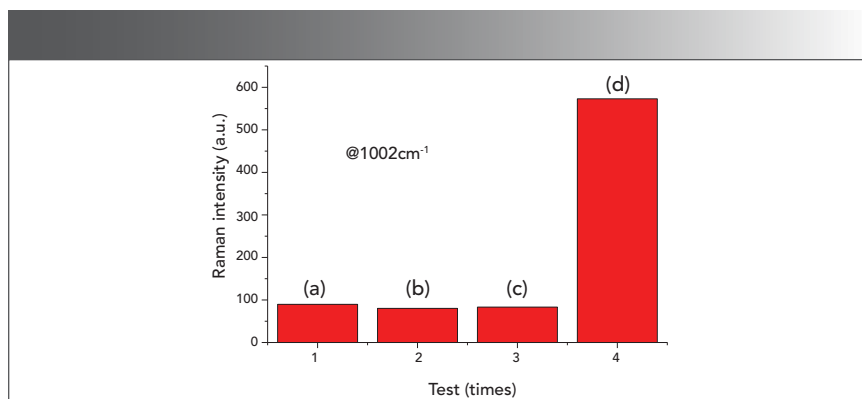


FIGURE 7: SERS intensity of mixture at 1002 cm⁻¹.

First, we centrifuged the mixed solution at a high speed for 20 min and removed the supernatant for detection. The results as shown in Figure 6b indicate that there was no signal of scopolamine. The signal intensity of promethazine greatly changed, indicating that the concentration of promethazine changed accordingly. However, the signal intensity of promethazine in the supernatant

increased because the relationship between concentration and signal intensity in the higher concentration range is not necessarily consistent. This is mainly because of the intensity saturation effect in SERS detection.

After the first centrifugation, the supernatant was again mixed with concentrated silver sol and prepared for the second centrifugation. After the second centrifu-

gation, the supernatant was removed for testing, and the results are shown in Figure 6c. The 1034 cm⁻¹ signal intensity for promethazine changed, indicating that the concentration also changed, but the main peak at 1002 cm⁻¹ for scopolamine still did not appear. On this basis, we continued to centrifuge the supernatant mixture of the previous step, and the supernatant after centrifugation was detected, as shown in Figure 6d. The signal of scopolamine was finally detected, and the signal strength of promethazine was much weaker. At the concentration of the mixture according to the actual use ratio, it was finally detected that both existed in the spectrum.

In the mixed solution, according to the actual ratio, we selected 1002 cm⁻¹ so we can clearly see the change of the spectrum of scopolamine in the process, which is shown in Figure 6. Figure 7 displays the results in a column chart. Although the first three times have weak intensity, they are below the detection limit so they can be regarded as the absence of scopolamine. The fourth time is the success of the actual detection of scopolamine.

Conclusions

We used simple experimental conditions to identify the spectrum of a solution mixture and utilized the disadvantageous SERS detection conditions to create a means of separating mixtures. This solves the problem that the strong adsorption component in the mixture can inhibit the weak adsorption component in the Raman spectrum. It should be noted that in the process of continuous centrifugation, the mixed solution is diluted to a certain extent. Although the relative concentration ratio of scopolamine is increasing, the concentration of scopolamine itself is decreasing, and therefore, the number of centrifugations needs to be properly controlled. The amount of silver sol used for centrifugation also requires optimization. Compared with other methods of separating mixtures, the procedure described herein is simple, and it is not only a feasible new method for the SERS detection of solution mixtures, but also for a rapid screening of new alternative drugs.

Acknowledgments

This work was supported by the National Natural Science Foundation of China(Grant No. 31871873), Inner Mongolia University for the Nationalities (Grant No. NMDYB18006), and the Inner Mongolia Autonomous Region Natural Science Foundation of China (Grant No. 2018LH08055).

Conflicts of Interest

There are no conflicts to declare.

References

- (1) M.K. Bohm and H.B. Clayton, *J. Adolesc. Health* **66**, S130 (2020).
- (2) J. Valentin, T. Mateo, M. Mariana, S. Virginie, S. Anne-Marie, L. Denis, S. Anaïs, L. Virginie, B. Fabrice, A. Serge, and R. Gerald, *Drug Test. Anal.* DOI:10.1002/dta.2745 (2020).
- (3) Q-T. Akram and S. Mostafa, *Gene* **724**, 144–153 (2020).
- (4) S. Kelly, *Crit. Public Health* **30**, 68–78 (2020).
- (5) K. Julia, W. Sophia, R. Francois, S. Norbert, B. Matthias, and W. Elisa, *Drug Alcohol Depend.* **205**, 107593 (2019).
- (6) B. Valentina, C. Ciro, M. Angelo, G.I.L. Francesco, P. Matteo, and M. Icro, *Heroin Addict. Relat. Clin. Probl.* **21**, 5–16 (2019).
- (7) G. Yong-Long, Z. Yang, C. Jiang-Peng, W. Sheng-Bing, C. Xing-Hui, Z. Yan-Chun, et al., *Acupunct. Med.* **35**(5), 366–373 (2018).
- (8) L. Yixin, X. Baijuan, L. Rongrong, Y. Dan, W. Yanlin and L. Wenmei, *Neuroreport* **28**, 654–66 (2017).
- (9) Z. Denghui, Z. Dengke, D. Huiqiong, Z. Xuehui, Q. Jinping, S. Hongxian, X. Xiaojun, W. Xuyi and H. W. Chin, *J. Drug Depend.* **15**, 35–39 (2006).
- (10) Z. Xuhui, W. Xuyi, L. Jun and H. Wei, *Chin. J. Clin. Psychol.* **19**, 285–288 (2011).
- (11) S. Wenwen, W. Qing, Z. Jianbin, P. Wenkai, Z. Jiawen, Y. Weiting, H. Qianyu, C. Deniz, and Z. Wenhua, *Front. Psychiatry* **10**, 888 (2019).
- (12) C. Daniel, O. Jeff, and M. Sarah, *Int. J. Drug Policy* **46**, 146–155 (2017).
- (13) C.P. Fang, S.C. Wang, H.H. Tsou, R.H. Chung, Y.T. Hsu, S.C. Liu, H.W. Kuo, T.H. Liu, A.C.H. Chen, and Y.L. Liu, *J. Hum. Genet.* **65**, 381–386 (2020).
- (14) W.W. Shen, Q. Wang, J.B. Zhang, W.K. Ping, J.W. Zhang, W.T. Ye, Q.Y. Hu, D. Cerci, and W.H. Zhou, *Front. Psychiatry* **10**, 888 (2019).
- (15) L. Bao, S. Han, X.Y. Sha, H. Zhao, Y.P. Liu, D.Y. Lin, and W. Hasi, *J. Spectrosc.* **2019**, 7458371 (2019).
- (16) J. Langer, D.J. de Aberasturi, J. Aizpurua, R. A. Alvarez-Puebla, B. Auguie, J.J. Baumberg, G.C. Bazan, S.E.J. Bell, A. Boisen, et al., *ACS Nano* **14**, 28–117 (2020).
- (17) R. Pilot, R. Signorini, C. Durante, L. Orian, M. Bhamidipati, and L. Fabris, *Biosensors-Basel* **9**, 57 (2019).
- (18) B.N.J. Persson, *Chem. Phys. Lett.* **82**, 561–565 (1981).
- (19) J. Faulds, R.E. Littleford, D. Graham, G. Dent, and W.E. Smith, *Anal. Chem.* **76**, 592–598 (2004).
- (20) C. Caro, P. Quaresma, E. Pereira, et al., *Nanomaterials* **9**, 256 (2019).
- (21) J. Langer, D.J. de Aberasturi, J. Aizpurua, et al., *ACS Nano* **14**, 28–117 (2020).
- (22) N. Leopold and B. Lendl, *J. Phys. Chem. B.* **107**, 5723–5727 (2003).
- (23) C. Carlos, J.S. Maria, F. Victorino, C. Alejandro, Z. Paula and G. Francisco, *Sens. Actuator B-Chem.* **228**, 124–133 (2016).
- (24) K. Kneipp, Y. Wang, H. Kneipp, et al., *Phys. Rev. Lett.* **78**, 1667–1670 (1997).
- (25) A.C. Sara, H. Szushen, R.G. Benito, et al., *Angew. Chem.-Int. Edit.* **48**, 5326–5329 (2009).
- (26) R.A. Sulk, R.C. Corcoran and K.T. Carron, *Abstr. Pap. Am. Chem. Soc.* **211**, 333–ANYL (1996).
- (27) K.J. Si, P.Z. Guo, Q.Q. Shi. and W.L. Cheng, *Anal. Chem.* **87**, 5263–5269 (2015).
- (28) X. Lin, W.L.J. Hasi, X.T. Lou, S. Han, D.Y. Lin and Z.W. Lu, *Anal. Methods* **7**, 3869–3875 (2015).
- (29) S.Z. Weng, M.Q. Qiu, R.L. Dong, F. Wang, L.S. Huang, D.Y. Zhang and J.L. Zhao, *Spectrosc. Acta Pt. A-Molec. Biomolec. Spectr.* **200**, 20–25 (2018).
- (30) H. Zhao, W. Hasi, L. Bao, Y.P. Liu, S. Han and D.Y. Lin, *J. Raman Spectrosc.* **49**, 1469–1477 (2018).
- (31) L. Gaft and L. Nagi, *Opt. Mater.* **30**, 1739–1746 (2008).
- (32) Y.Q. Qin, X.H. Ji, J. Jing, H. Liu and H.L. Wu, *Colloids Surf. A* **372**, 172–176 (2010).

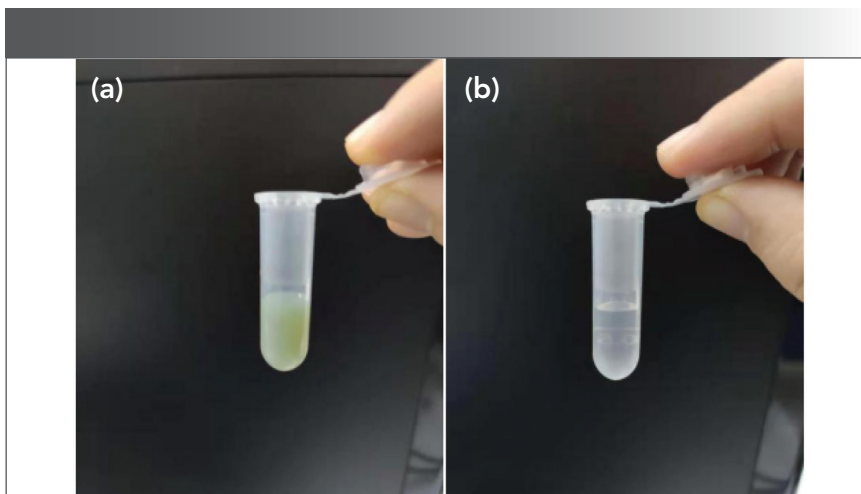


FIGURE 8: (a) Silver sol before centrifugation, and (b) silver sol after centrifugation.

Wuliji Hasi is with the National Laboratory of Science and Technology at the Harbin Institute of Technology in Harbin, China. **Lin Bao** is with the National Laboratory of Science and Technology at the Harbin Institute of Technology in Harbin, China, and the College of Physics and Electronic Information at the Inner Mongolia Universities for Nationalities. **Siqingawa Han** is with the Affiliated Hospital at Inner Mongolia University for the Nationalities. Direct correspondence to Wuliji Hasi at hasiwuliji19@163.com •

Enhanced Raman and Mid-Infrared Spectroscopic Discrimination of Geographical Origin of Rice by Data Mining and Data Fusion

Min Sha, Dongdong Gui, Peng Li, Zhengyong Zhang,
Yu Huang, Minqin Jiang, and Jun Liu

Data mining and fusion of Raman and mid-infrared (mid-IR) spectra was studied to improve the identification ability for geographical origins of rice. Relative standard deviation (RSD) analysis can predict whether there are outlier Raman spectra. Hierarchical clustering analysis (HCA) can find out the potential outlier data, and then RSD analysis can finally determine the outlier data. The recognition accuracy of the model built by eliminating the outlier data was higher than that of the model using all the data. The identification accuracy of the data fusion model was 97.8%, 4.5% higher than that of the Raman and mid-IR models. The model was further applied to identify the geographical origins of 10 japonica rice varieties, with an accuracy of 96.7%. A combination of data mining and data fusion can enhance the discrimination ability for the geographical origin of rice using a combination of Raman and mid-IR spectroscopy.

Rice is one of the most important cereal crops. It is rich in protein, fat, carbohydrates, and other nutrients (1,2). Its quality is influenced by many factors, such as genetics, growing conditions, and processing (3). With living standards improving, geographical indication products are becoming more popular among consumers because of their better quality. Meanwhile, the phenomenon of confusion or adulteration appears, bringing unfair economic benefits to the fraudsters and destroying the credibility of consumers to producers (4). Therefore, it is necessary to develop a reliable tool to identify the geographical origin of rice for consumers, honest producers, retailers, and governments.

Sensory identification (5), biological identification (6,7), chemical identification (stable isotope [8,9]), trace elements (10,11), volatile components (12–14), and other technologies have been widely used to identify the geographical origin of rice. Among them, cheap and fast spectral technologies, combined with pattern recognition methods, are becoming more pop-

ular, and are generally used in the analysis of multicomponent samples.

The literature reports the application of Raman spectroscopy in identifying the geographical origin of rice. For example, Hwang and others reported the identification of Korean and imported rice with the recognition accuracy of 98% (15). Kim and co-authors identified rice that came from China and Korea with the recognition accuracy of 96% (16). Feng and others identified rice that originated from different provinces in China with the highest recognition accuracy of 100% (17,18). Most of the rice samples used in these studies are shelled rice grains, so only the information of components outside the rice grains are collected. It is well known that the weight percentages of carbohydrates, protein, fat, and water in rice grains are about 70–80%, 7–8%, 1–2%, and 11–12%, respectively, and the distribution of the components in rice grains is inhomogeneous (19). Besides, the rice processing technology, such as polishing, will cause differences on the surface

of rice. Therefore, the Raman spectra obtained are insufficient to reflect the information of the whole composition of rice. To analyze the rice grains accurately, they need to be pulverized and sieved to obtain the rice flour sample as evenly as possible (20). In addition, the existing literature focused on the identification of geographical origins and varieties of rice and other inhomogeneous products mainly obtain the spectral information based on the average of two or three measurements (21). The possibility of outlier data caused by large fluctuations is not taken into account, and the accuracy of the data by taking the average is unknown. To make the obtained spectra reflect the sample information more comprehensively, it is necessary to collect enough spectra and eliminate the outliers.

As the growing environment changes, so does the content or structure of components in rice, thus the position and intensity of the absorption peaks of infrared spectra are different, and these differences can be used to reflect the regional characteristics of rice products (22). Xia and colleagues used near-infrared spectroscopy (NIR) and Fisher's linear discriminant to discriminate Xiangshui rice with the accuracy of 100% (23). In the discrimination of non-Xiangshui rice originated from nine provinces, 92.3% of the modeled samples were classified correctly, and 90.9% of the validated samples were correctly discriminated. Compared with the NIR spectrum, the absorption peak of the mid-IR spectrum is usually sharper, with good resolution and high peak value. Nowadays, the updated mid-IR spectrometer in the market does not require sample preparation, greatly saving testing time, and is an ideal fast detection technique. However, the application of mid-IR spectroscopy in identifying the geographical origin of rice is rare.

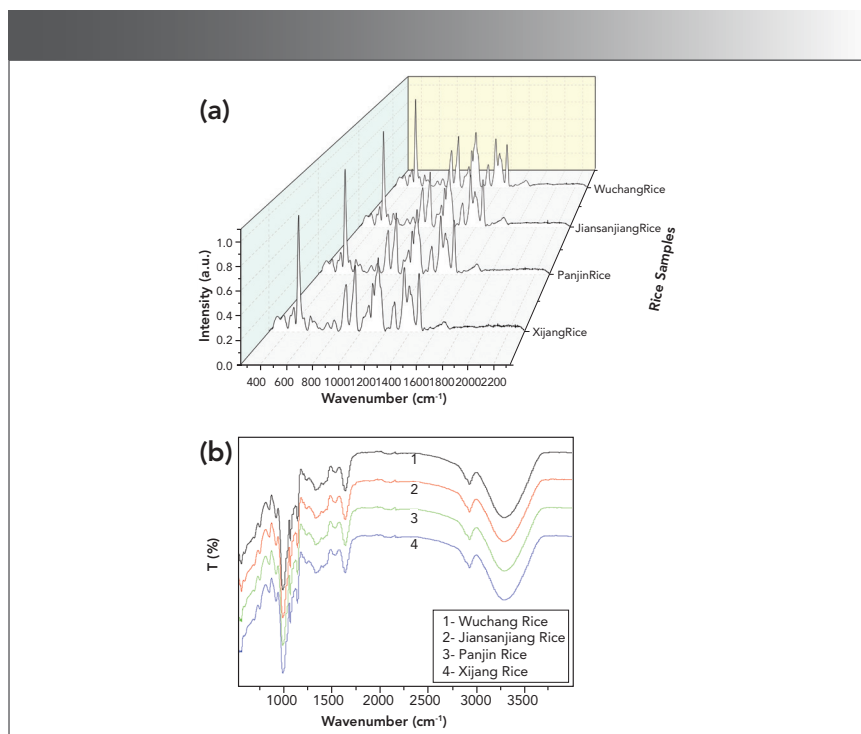


FIGURE 1: Typical (a) Raman and (b) mid-IR spectra of the four kinds of rice after pretreatment.

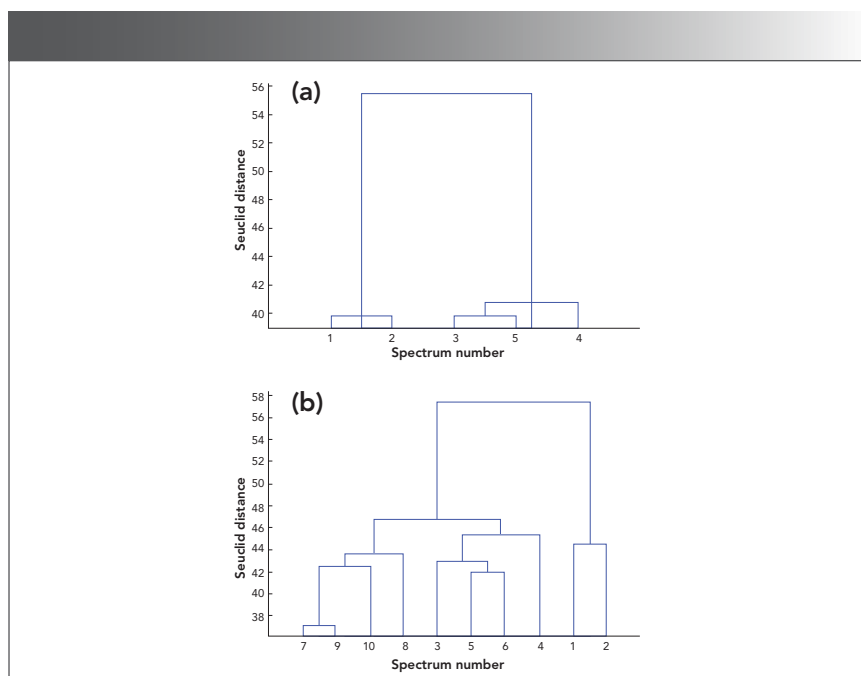


FIGURE 2: Clustering trees for (a) the five Raman spectra of sample 1 of Xijiang rice in position 2, and (b) the ten Raman spectra of Xijiang rice in position 2 (spectra 1-5 refer to xj211-215 while spectra 6-10 refer to xj221-225 in Table I).

The above methods for identification of the geographical origin of rice are mostly based on a single

technique that can not reflect the composition information of rice sufficiently. For example, artificial falsi-

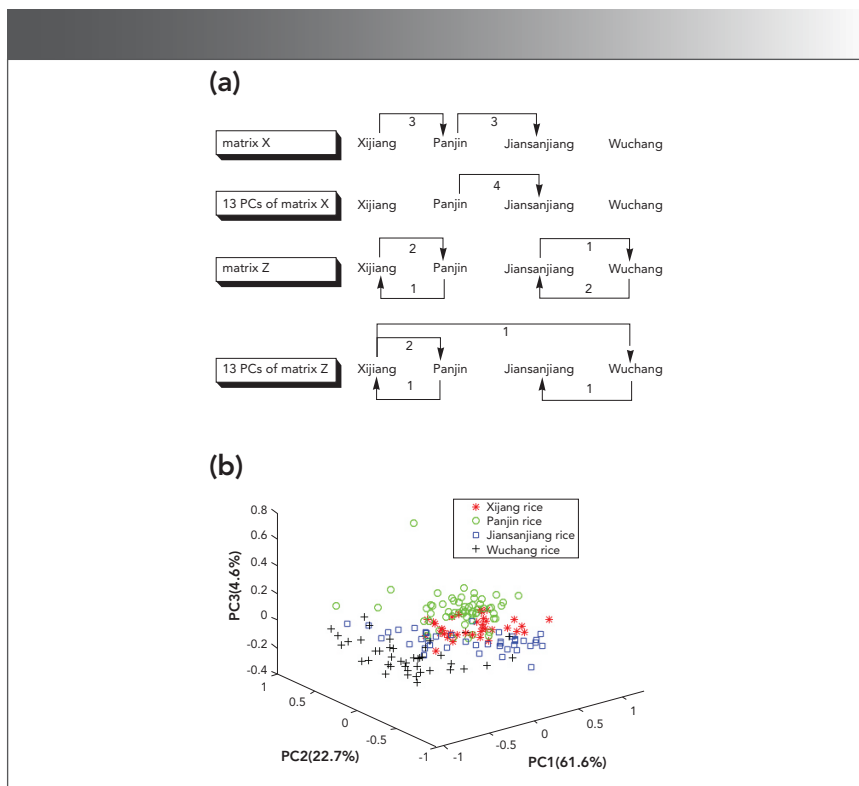


FIGURE 3: (a) Details of misclassified rice samples by Raman spectroscopy; (b) Distribution of rice samples in the multidimensional principal component analysis (PCA) space formed by the first three PCs of mid-IR spectra.

fication of specific chemical indicators will cause serious interference to chemical identification methods, so the reliability of identification results is poor. Moreover, the existing identification methods are commonly aimed at rice samples grown in different countries or different provinces in the same country. The geographical areas are far apart from each other, making identification relatively easy. There have been many reports on the application of data fusion technology in food quality detection (24,25). Sun and others established a model for identifying official rhubarb using NIR spectroscopy and mid-IR spectroscopy, using data fusion strategies to improve the classification model and allow the correct classification of all the samples (26). Hohmann and associates can effectively distinguish a total of 205 tomato samples of nine varieties from seven farms with

an accuracy rate of 95 to 100% by combining proton nuclear magnetic resonance, mid-IR spectroscopy, and isotope ratio mass spectrometry (27). According to the literature, data fusion of Raman and infrared spectra for geographical identification of rice is rarely reported.

Therefore, in this work, rice products grown in four geographical regions (Xijiang, Panjin, Jiansanjiang, and Wuchang) in northeast China were taken as representative examples to develop an excellent identification model. Rice samples were refined, crushed, and screened to obtain relatively uniform rice flour samples. Raman and mid-IR spectra were obtained. Outlier Raman spectra were eliminated. A model was established by support vector machine based on data fusion of Raman and infrared spectra aimed at improving the identification accuracy and reliability for geographical

origins of rice. Finally, the promotion and application value of the established method and model were studied in 10 kinds of rice.

Materials and Methods

Samples

For this experiment, 10 types of geographical indication rice products were collected from different areas of China, as seen in Figure S1 (Supplemental figures and tables, designated by an S before their number, can be found with this article on the *Spectroscopy* website). Fangzheng rice, Jiansanjiang rice, Wuchang rice, and Xiangshui rice were all grown in Heilongjiang province. Yanbian rice and Xijiang rice were both grown in Jilin province. Xinghua rice and Heheng rice were grown in Jiangsu province. Panjin rice was grown in Liaoning province. Yutai rice was grown in Shandong province. All of the rice samples were cultivated in 2017 and 2018, and collected in different planting areas to ensure they are representative of the samples. Xijiang, Panjin, Jiansanjiang, Wuchang, Xiangshui, Yanbian, Fangzheng, Heheng, Xinghua, and Yutai rice were collected from 18, 30, 21, 21, 30, 15, 33, 21, 21, and 33 positions, respectively. Two samples were collected in each position, each sample took about 2 kg of rice, and all the samples were japonica rice with specific varieties.

Instruments and Equipment

Rice milling process mainly used paddy huller (NA12345) and rice mill (NA-JCB) which were both produced by Kemai Instrument Co., Ltd. A vertical grinder (15B, Baling Electric Appliance Co., Ltd.) was used to crush rice samples, and the diameter of stainless steel sieve in it was 0.6 mm. Raman spectra were recorded using a portable laser Raman spectrometer (Prott-ezRaman-d3, Enwave Optronics), samples were simply transferred on a quartz glass with 2 mm thick. Mid-IR spectra were recorded using an attenuated total reflectance (ATR) Fourier transform infrared

spectrometer (Nicolet IS-10, Thermo Fisher Scientific).

Methods

Sample Preparation

Rice samples were processed according to the requirements of the first grade japonica rice in GB/T 1354-2018. Then, 20 g of each grain sample was slowly added to the grinder within half a minute and crushed for 2 min to ensure complete crushing. The rice flour obtained was screened by 100 and 140 mesh sieves successively. Rice flour with the size of 100–140 mesh was stored in a freezer and balanced to room temperature in a dryer before spectral analysis.

Spectrum Collection

The parameters for Raman spectrum acquisition were as follows. The excitation wavelength of laser was 785 nm, the laser power was 450 mW, the temperature of the charge-coupled detector (CCD) detector was -85°C , the spectrometer operated from 250 to 2339 cm^{-1} with a resolution of 1 cm^{-1} , and the number of scans was three with each having an accumulation time of 4 s. Five replicated spectra were acquired at different positions for each sample. The total test time of a sample was about 2 min, including sample loading, testing (five times), spectrum saving, and desktop cleaning.

The parameters for the mid-IR spectrum acquisition were as follows: The spectrometer operated from 525 to 4000 cm^{-1} with a resolution of 0.4821 cm^{-1} , and each sample was scanned 32 times. An appropriate amount of rice flour was covered on the testing window and was compacted for test subsequently. All the samples were analyzed in triplicate. The total test time of a sample was about 2.5 min.

Data Analysis

To remove interfering and irrelevant information from the original spectral data, pretreatment should be done before data analysis. In this

work, Raman spectra and mid-IR spectra were denoised by a wden wavelet function (28), which eliminated the effect of scattering by multiplicative scatter correction (29), and normalized by the mapminmax function (30) successively. As Raman measurement was relatively interfered by the environment and instrument, relative standard deviation (RSD) analysis and hier-

archical clustering analysis (HCA) (31,32) were comprehensively applied to eliminate outliers. Then, the average Raman spectrum and mid-IR spectrum for each sample were taken as the representative spectra. Finally, a support vector machine (SVM) (33) was used to establish the model, with the radial basis function (RBF) (34) being used. In addition, Gamma and C parameters were op-

Results in just 5 minutes

No sample prep required

Up to 70% cost reduction

powered by **milestone**
connect

Time doesn't stand still. Neither do we.

Milestone's market-leading DMA-80 evo sets the standard for mercury analysis, offering more than double the productivity of traditional cold vapor techniques at a fraction of the cost per sample. Simple push-button operation and no sample prep provides built-in efficiency, generating accurate results in just 5 minutes.

Time in your lab is valuable. Let the DMA-80 evo help you make the most of it.

Call us today at 866.995.5100 or visit www.milestonesci.com/evo to learn more.



TABLE I: The detailed information for Xijiang rice

Sample Position	Sample 1				Sample 2			
	Spectrum Number	RSD ₁ ^a (%)	Outlier Spectrum	RSD ₂ ^b (%)	Spectrum Number	RSD ₁ ^a (%)	Outlier Spectrum	RSD ₂ ^b (%)
1	xj111-115	14.7	xj111,xj112	12.5	xj121-125	13.2	---	13.2
2	xj211-215	17.2	xj211,xj212	13.9	xj221-225	12.6	---	12.6
3	xj311-315	13.4	---	13.4	xj321-325	13.2	---	13.2
4	xj411-415	12.1	---	12.1	xj421-425	14.6	xj422	12.1
5	xj511-515	12.5	---	12.5	xj521-525	14.0	---	14.0
6	xj611-615	12.5	---	12.5	xj621-625	12.3	---	12.3
7	xj711-715	12.7	---	12.7	xj721-725	12.3	---	12.3
8	xj811-815	17.2	xj812, xj814	14.0	xj821-825	12.3	---	12.3
9	xj911-915	10.2	---	10.2	xj921-925	14.4	xj922, xj923	12.2
10	xj1011-1015	12.1	---	12.1	xj1021-1025	14.7	xj1023	12.6
11	xj1111-1115	12.4	---	12.4	xj1121-1125	10.9	---	10.9
12	xj1211-1215	11.8	---	11.8	xj1221-1225	13.9	---	13.9
13	xj1311-1315	12.8		12.8	xj1321-1325	13.8	---	13.8
14	xj1411-1415	14.5	xj1414, xj1415	12.2	xj1421-1425	13.3	---	13.3
15	xj1511-1515	13.4	---	13.4	xj1521-1525	11.7	---	11.7
16	xj1611-1615	11.3	---	11.3	xj1621-1625	17.4	xj1623, xj1624	14.0
17	xj1711-1715	12.4	---	12.4	xj1721-1725	10.9	---	10.9
18	xj1811-1815	12.1	---	12.1	xj1821-1825	14.5	xj1823	12.1

^a RSD value of all the data^b RSD value of the valid data

timized by a grid search technique within the region of 10^{-5} to 10^5 . The data of one sample of each sampling point was used as the training set, and the data of the another sample was used as the prediction set. All of the data preprocessing and model construction were based on Matlab 2019b.

Results and Discussion

Spectrum Analysis

Taking Xijiang, Panjin, Jiansanjiang, and Wuchang rice as examples that originated from three neighboring provinces in northeast China, the spectra of sample 1 in position 1 were pretreated and shown in Figure 1. The peaks of Raman spectra mainly located in the region of $251\text{--}1500\text{ cm}^{-1}$, especially located at 492, 878, 952, 1094, 1126, 1139, 1273,

1351, 1390, and 1474 cm^{-1} . Through RSD analysis, it was found that the bands with high stability of mid-IR spectra located at $578\text{--}4000\text{ cm}^{-1}$, and the peaks mainly occurred at 859, 928, 997, 1080, 1150, 1640, 2930, and 3290 cm^{-1} . Therefore, the data of these regions were adopted for subsequent analysis. As seen in Figure 1, the spectra of the four kinds of rice from different producing areas were highly similar which were difficult to be recognized by naked eyes.

Model Analysis

Geographical Identification of Rice by Raman Spectroscopy

In the region of $251\text{--}1500\text{ cm}^{-1}$, taking Xijiang rice as an example, RSD values of the five Raman spectra of each sample are shown in Table I. Because

of the fluctuation of instrument and environment, inhomogeneity of rice flour, and some man-made factors, the RSD values generally fluctuated below 14%. Among them, the RSD value of some rice samples were so large that there might be outlier data.

The HCA of five Raman spectra of each sample was performed to find out the possible outlier spectrum intuitively. Euclidean distance (35), standard Euclidean distance, city block distance, and the congruence coefficient (cosine) (36) were used as distance measures to quantify the similarity between spectra. Linkage methods, such as average linkage (37), single linkage, and complete linkage, were applied to construct the clustering tree (38). Taking sample 1 of Xijiang rice in position 2 for example, the values of cophenetic

VC Ultra

Acid Vapor Cleaning System

Savillex's VC Ultra Acid Vapor Cleaning System offers labs performing microwave sample preparation a safe, efficient and user-friendly alternative for cleaning microwave digestion vessels and other labware.

- › Large, fluoropolymer cleaning chamber can accommodate up to 40 microwave digestion vessels and covers
- › Customized digestion vessel cleaning racks minimize handling and acid exposure
- › Pre-programmed cleaning cycles eliminate method development



TABLE II: The results of models using various data

Number of the First Several PCs	Accumulated Contribution Rate ^a (%)	Recognition Accuracy ^a (%)	Total Recognition Time ^a (s)	Recognition Accuracy ^b (%)
13	80.1	95.6	2.4	85.6
19	85.4	95.6	3.0	86.7
27	90.4	92.2	3.2	88.9
39	95.1	92.2	3.6	91.1
51	98.1	93.3	4.1	91.1
179	100.0	93.3	9.4	91.1

^a model using the data after eliminating the outlier spectra^b model using all the data**TABLE III:** Identification results of models using different PCs

Number of the First Several PCs	Accumulated Contribution Rate (%)	Recognition Accuracy (%)	Total Recognition Time (s)
2	84.3	54.4	1.8
3	89.0	71.1	1.9
4	92.0	78.9	1.9
6	96.1	83.3	2.0
9	98.2	91.1	2.1
13	99.1	94.4	2.4
179	100.0	93.3	9.4

correlation coefficient for different methods were calculated and shown in Table SI. The best created clustering tree using seculidean distance measure and average linkage method was shown in Figure 2a. Spectra 1 and 2 had high similarity and were clustered together while spectra 3–5 clustered together. The distinction between spectra 1 and 2 and spectra 3–5 was very obvious. However, it was still difficult to judge the outlier data.

The HCA was further carried out on the ten spectra of Xijiang rice in position 2, and the results were shown in Figure 2b. Spectra 1 and 2 were significantly different from the other eight spectra, indicating that they were the potential outliers. After eliminating spectra 1 and 2, RSD value of the remaining three Raman spectra of sample 1 in position 2 was 13.9% which was within the fluctuation range (below 14%),

confirming that spectra 1 and 2 were the outlier data. Spectra 3–8 in Figure 2b were mixed together indicating that the difference between the two rice samples in the same position was small. The above research results showed that RSD analysis can predict whether outliers exist, HCA analysis can find out the potential outliers, and the outliers can be finally identified and verified by RSD analysis. Combination of RSD analy-

sis and HCA provides an accurate and reliable method to eliminate the outliers.

The same analysis of Xijiang rice in the remaining 17 positions was processed, and the outlier data found are shown in Table I. It was found that outlier data exist in all the rice samples which RSD values were over 14%, and the RSD values after eliminating the outlier data were all less than 14%, indicating that the existence of outlier data can be preliminarily judged by the fluctuation range of the RSD value. The 15 outlier spectra in Table I should be eliminated for subsequent modeling. Furthermore, after analyzing the Raman spectra of Panjin, Jiansanjiang, and Wuchang rice, it was found that there were seven, four, and one outlier spectra, respectively (Tables SI–SIV)

Average of Raman spectra after eliminating outlier data were taken as the representative spectra for each sample, values of the Raman absorbance were taken as independent variables, and the geographical origin was used as the dependent variable. Thus, matrix X (180×1250) and matrix Y (180×1) were formed. The number of samples was 180, and 1250 was the number of independent variables, along with one dependent variable. The recognition accuracy of the model based on matrix X was 93.3%, and the total recognition time was 54.9 s. Another prediction model was established by using the data without eliminating the outlier spectra, the recognition rate was 91.1%, and the recognition time was 55.1 s.

Taking into account the relevant variables will influence the efficiency of the model, and the principal component analysis (PCA) can extract the main information of the data, so PCA of matrix X was carried out before modeling, and the results were shown in Table II. The accumulated contribution rate of the first 179 principal components (PCs) was 100.0%, demonstrating that the 179 PCs can represent the overall information of

matrix X. The recognition accuracy of the model using the 179 PCs was consistent with the result of matrix X, but its value was not the largest in Table II, indicating that there are some useless information in the first 179 PCs. When the numbers of PCs were 13, 15, 16, 18–21, and 24, the recognition accuracy was the highest (95.6%), and the total recognition time was 2.4–3.0 s, which were both better than those

of the model built with matrix X. The misidentified samples were shown in Figure 3a. When matrix X was used, there were six wrongly classified samples. Three samples of Xijiang rice were classified as Panjin rice, three samples of Panjin rice were classified as Jiansanjiang rice. When the numbers of PCs were 13, 15, 16, 18–21, and 24, four samples of Panjin rice were wrongly classified as Jiansanjiang

BWTEK
A Metrohm Group Company



Portable Raman Analyzer for Measurements Through Opaque Packaging

The STRam® provides easy identification of materials through a variety of packaging and barrier layers utilizing 785nm or 1064nm wavelengths!

Learn More about the STRam
www.bwtek.com/STRam

rice. It could be seen that the results varied greatly using different data, and the recognition accuracy of the model built by eliminating the outlier data was always higher than that of the model using all the data (Table II).

Geographical Identification by Mid-IR Spectroscopy

Mid-IR spectra of 180 samples of four kinds of rice were averaged as the representative spectra for each sample, values of the transmittance of mid-infrared spectra were taken as independent variables, and the geographical origin was used as dependent variable. Thus, matrix Z (180×7100) and matrix Y (180×1) were formed, with 7100 being the number of independent variables. The recognition accuracy of the model based on matrix Z was 93.3%, and the total recognition time was 307.4 s. PCA was then carried out on matrix Z, the results of the identification model using different PCs were shown in Table III. With the increase of the number of PCs, total recognition time increased when the number of PCs was between 13 and 15 and identification accuracy was 94.4%, which was the largest in Table III and much better than the results using matrix Z. When the identification accuracy was 94.4%, five samples were wrongly identified as can be seen in Figure 3a. Distribution of rice samples in the space formed by the first 3 PCs was shown as Figure 3b. Panjin rice was close to Xijiang and Jiansanjiang rice, some samples of Xijiang and Jiansanjiang rice were crossed together, and a few samples of Jiansanjiang and Wuchang rice overlapped. These samples were easy to be misjudged during identification, which explained why the recognition accuracy was only 71.1% when the number of PCs was three.

Identification Results After Data Fusion

Transitions between vibrational and rotational levels of chemical bonds

or functional groups absorb infrared light, so the infrared spectrum can reflect the information of functional groups or chemical bonds contained in molecules. Besides, infrared absorption takes place only when there is a change of dipole moment. Raman spectrometer analyses the scattered light with different frequency from the incident light to obtain the information of molecular structure. Different from infrared spectrum, both polar molecules and nonpolar molecules can produce Raman spectrum. Therefore, if the two spectra is integrated, the information representing the composition of rice can be more comprehensive. According to the above experimental results, the misclassified samples corresponding to the best identification accuracy of Raman and mid-IR spectroscopy were entirely different, so data fusion of the two spectra can play a complementary role.

Low-level fusion of data was conducted first. Matrix X (180×1250) and matrix Z (180×7100) were fused into matrix M (180×8350) according to the method shown in Figure S2 (taking sample 1 of Xijiang rice in position 1 as an example). It was found that the recognition accuracy of the model using matrix M was 97.8% and the recognition time was 387.3 s. Data fusion by this method had achieved ideal recognition accuracy, but the recognition took a long time.

To overcome the low recognition efficiency, mid-level data fusion was used. According to the results in Table II and Table III, 13, 15, 16, 18–21, and 24 PCs corresponding to the highest identification accuracy of Raman spectroscopy were selected respectively, and new data matrices were constructed by combined with 13 and 15 PCs corresponding to the highest identification accuracy of mid-IR spectroscopy. The newly established classification models had the highest recognition accuracy of 97.8% (Table SV), which was

4.5% higher than that of Raman and infrared spectroscopy. One sample of Xijiang rice was wrongly identified as Wuchang rice while one sample of Wuchang rice was wrongly identified as Jiansanjiang rice.

Promotion and Application of Data Mining and Data Fusion Technology

The promotion and application of data mining and data fusion technology were further studied. Xiangshui rice, Yanbian rice, Fangzheng rice, Heheng rice, Xinghua rice, Yutai rice, and the above studied four kinds of rice were identified together. The matrix of Raman spectra data was 486×1250 , the identification accuracy was 91.8%, and the identification time was 430.9 s. The matrix of mid-IR spectra data was 486×7100 , the identification accuracy was 91.8%, and the identification time was 2497.7 s, the model was time-consuming and its identification accuracy was not ideal. To improve the recognition accuracy and efficiency of the model, data mining (Tables SVI–SXI) and mid-level data fusion method was adopted. When the number of Raman PCs was 40 and the number of infrared PCs was 35, the identification accuracy of the ten kinds of rice was 96.7%, and the identification time was 40.1 s. The results were relatively ideal and consistent with expectations.

Conclusion

Taking Xijiang rice, Panjin rice, Jiansanjiang rice, and Wuchang rice as examples, this paper explored the influence of data fusion of Raman spectra and mid-IR spectra on the geographical identification model. First of all, rice samples were processed, crushed, and screened, and rice flour sized between 100–140 mesh were obtained. Second, Raman spectra and infrared spectra of each sample were collected at 5 measurement positions and in triplicate respectively. The collected spectra were pretreated by denoising, multivariate scattering correction and normalization successively. RSD analysis and HCA were applied to detect of outliers from

Raman data of each sample. Then, the Raman spectra and mid-IR spectra of each sample were averaged respectively. Finally, the geographical identification models were established by support vector machine using Raman data, mid-IR data and the fusion of the two data. The results showed that RSD analysis can predict whether there are outliers, HCA analysis can find out the potential outlier data, and then RSD analysis can finally determine the outlier data, the comprehensive application of RSD analysis and HCA provides an accurate and reliable method to eliminate the outliers. In addition, data fusion realized complementarity of Raman and mid-IR spectra information, and the accuracy of the established model was 97.8%, which was 4.5% higher than that of Raman data and mid-IR data. The data fusion method explored in this paper provided more accurate and reliable data for identifying geographical origins of rice quickly. Besides, the identification accuracy of 10 kinds of rice with close geographical location was 96.7%, which was higher than 90.0%, demonstrating that the data pretreated method and the data fusion model proposed were effective and worthy popularization.

Supplemental Information



Additional information for this article, including Figures S1 and S2, as well as Tables SI through SXI, is available online at <https://www.spectroscopyonline.com/>. Scanning the QR code at left will link directly to this information.

Conflicts of Interest

The authors have no conflicts of interest.

Acknowledgments

This work was supported by the Natural Science Foundation of Jiangsu Province [grant number BK20180816]; the Natural Science Research of Jiangsu Higher Education Institutions of China [grant number 17KJD550001]; and the National Natural Science Foundation of China [grant number 61602217].

References

- (1) Y.B. Monakhova, D.N. Rutledge, A. Roßmann, et al., *J. Chemometrics* **28**(2), 83–92 (2014).
- (2) S.Y. Park, J.K. Kim, J.S. Jang, et al., *Food Sci. Biotechnol.* **24**(1), 225–231 (2015).
- (3) K.L. Bett-Garber, R.J. Bryant, C.C. Grimm, et al., *Cereal Chem.* **94**(3), 602–610 (2017).
- (4) H.B. Zhu, Y.Z. Wang, H. Liang, et al., *Talanta* **81**(1–2), 129–135 (2010).
- (5) G.A. Camelo-Méndez, B.H. Camacho-Díaz, A.A. Villar-Martínez, et al., *J. Sci. Food Agric.* **92**(13), 2709–2714 (2012).
- (6) M. Ashfaq and A.S. Khan, *Russ. J. Genet.* **48**(1), 53–62 (2012).
- (7) M.M. Voorhuijzen, J.P. van Dijk, T.W. Prins, et al., *Anal. Bioanal. Chem.* **402**(2), 693–701 (2012).
- (8) K. Ariyama, M. Shinozaki, and A. Kawasaki, *J. Agric. Food Chem.* **60**(7), 1628–1634 (2012).
- (9) R.A. Lagad, S.K. Singh, and V.K. Rai, *Food Chem.* **217**, 254–265 (2017).
- (10) G. Li, L. Nunes, Y.J. Wang, et al., *J. Environ. Sci.* **25**(1), 144–154 (2013).
- (11) J. Promchan, D. Günther, A. Siripinyanon, et al., *J. Cereal Sci.* **71**, 198–203 (2016).
- (12) R.J. Bryant and A.M. Mcclung, *Food Chem.* **124**(2), 501–513 (2011).
- (13) D.K. Lim, C. Mo, D.K. Lee, et al., *J. Food Drug Anal.* **26**(1), 260–267 (2018).
- (14) D.S. Yang, K. Lee, and S.J. Kays, *J. Sci. Food Agr.* **90**(15), 2595–2601 (2010).
- (15) J. Hwang, S. Kang, K. Lee, et al., *Talanta* **101**, 488–494 (2012).
- (16) Y. Kim, S. Lee, H. Chung, et al., *J. Raman Spectrosc.* **40**(2), 191–196 (2009).
- (17) X. Feng, Q. Zhang, P. Cong, et al., *Talanta* **115**, 548–555 (2013).
- (18) L. Zhu, J. Sun, G. Wu, et al., *J. Cereal Sci.* **82**, 175–182 (2018).
- (19) S. Chaiwanichsiri, D. Thumrongchote, T. Suzuki, et al., *Res. J. Pharm. Biol. Chem. Sci.* **3**(1), 150–164 (2012).
- (20) M. Sha, D.D. Gui, Z.Y. Zhang, et al., *J. Food Meas. Charact.* **13**(3), 1705–1712 (2019).
- (21) D. Ballabio, E. Robotti, F. Grisoni, et al., *Food Chem.* **266**, 79–89 (2018).
- (22) D. Cozzolino, *Food Res. Int.* **60**, 262–265 (2014).
- (23) L.Y. Xia, S.G. Shen, Z.H. Liu, et al., *Spectrosc. Spect. Anal.* **33**(1), 102–105 (2013).
- (24) E. Borràs, J. Ferré, R. Boqué, et al., *Anal. Chim. Acta* **891**, 1–14 (2015).
- (25) L. Wang, D. Liu, H. Pu, et al., *Food Anal. Method* **8**(2), 515–523 (2015).
- (26) W.J. Sun, X. Zhang, Z.Y. Zhang, et al., *Spectrochim. Acta A* **171**, 72–79 (2016).
- (27) M. Hohmann, Y. Monakhova, S. Erich, et al., *J. Agr. Food Chem.* **63**(43), 9666–9675 (2015).
- (28) M. Sha, D. Zhang, Z.Y. Zhang, et al., *J. Raman Spectrosc.* **51**, 702–710 (2020).
- (29) I. Tomas and N. Tormod, *Appl. Spectrosc.* **42**, 1273–1284 (1988).
- (30) H.A.H. Naji, Q.J. Xue, K. Zheng, et al., *Sensors* **20**(8), 2331 (2020).
- (31) C.M. Farrelly, S.J. Schwartz, A.L. Amodeo, et al., *J. Res. Pers.* **70**, 93–106 (2017).
- (32) S.C. Johnson, *Psychometrika* **3**, 241–254 (1967).
- (33) S.R. Amendolia, G. Cossu, M.L. Gandu, et al., *Chemom. Intell. Lab. Syst.* **69**, 13–20 (2003).
- (34) R.M. Balabin and S.V. Smirnov, *Talanta* **85**, 562–568 (2011).
- (35) L. He, B. Agard, and M. Trepanier, *Transportmetrica A: Transport Sci.* **16**(1), 56–75 (2020).
- (36) L.Z. Hong, Q.L. Bao, L.T. Yue, et al., *Food Chem.* **145**, 625–631 (2014).
- (37) H.S. Zwick and S.A.S. Syed, *Appl. Econ. Lett.* **24**(7), 472–476 (2017).
- (38) M. Sha, Z.Y. Zhang, D.D. Gui, et al., *Food Anal. Method* **10**, 3415–3423 (2017).

Min Sha, Zhengyong Zhang, Yu Huang, Minqin Jiang, and Jun Liu are with the School of Management Science and Engineering at Nanjing University of Finance and Economics in Nanjing, China. **Dongdong Gui** is with the College of Civil Aviation at Nanjing University of Aeronautics and Astronautics in Nanjing, China. **Peng Li** is with the School of Food Science and Engineering, Nanjing University of Finance and Economics in Nanjing, China. Direct correspondence to: shaminjingjing@163.com. •

The 2021 Employment and Salary Survey: Covid-19 and the New Virtual World

Jerome Workman, Jr.

Last year was undoubtedly a year of significant challenges and change—Covid-19, working from home, masks, social distancing, and virtual connections to laboratories and conferences. This year's *Spectroscopy* salary and employment survey explores the impact on spectroscopic scientists from around the world and their reactions, responses, and outlook.

As always, we report on overall salary trends and how they compare to past years, referring all the way back to the 2001 survey. But unlike previous reports about *Spectroscopy* salary surveys, which focused heavily on the numerical details of the salary data (1,2), this year we looked beyond the numbers to focus more on broader trends of workplace satisfaction and career attitudes. We asked about job security and solicited respondents' outlook for a future working in this challenging and technically complex field. We inquired about what spectroscopy professionals consider their greatest workplace concerns. We asked how many respondents are searching for new opportunities and why—and we looked at the effects caused by working in a Covid-19 environment in the workplace. We also asked respondents for their outlook for the remainder of 2021. In sum, we looked into multiple factors of the current and future employment environment.

The Overall Picture

As would be expected, we found that nearly all professionals working in the field of spectroscopy are more concerned than usual about the security of their jobs and incomes, given the Covid-19 pandemic. Nevertheless,

respondents are fairly optimistic about the coming year. Nearly 64% of respondents expect the economy to recover to its previous levels during 2021, and 65% believe their job situation will improve during 2021. There is also strong confidence among our respondents (60%) that their own organizations will improve their revenue streams and organizational health in 2021.

Nevertheless, one-third of respondents (35%) indicated that they are interested in seeking a new employment opportunity for reasons unrelated to the pandemic, while 44% say they do not want to leave their current position even if a promising new opportunity was presented.

The Covid-19 Effect

As we all know, the Covid-19 declared pandemic resulted in dramatic changes in working conditions throughout the world. Since the pandemic was officially declared in March of 2020, nearly one in five (15%) respondents were either laid off or furloughed; over half (50.5%) have limited or no access to their laboratories; and, more alarmingly, 34% say they are struggling to stay positive during this globally impacting situation.

Nearly all types and sizes of organizations and their operations have been

seriously challenged by the pandemic, as facilities have been closed or have implemented severely restricted access. This has forced the adoption of online or virtual corporate and university classes, meetings, and scientific and business conferences—a mandated requirement in nearly every situation. According to our respondents, the business downturn caused by the pandemic has resulted in nearly two-thirds (60%) of organizations downsizing specifically due to the Covid-19 lockdown, with an additional 25% downsizing for reasons not directly related to Covid-19. It is noteworthy that 10% of respondents say their work functions were offshored during this period.

In spite of the challenges of the shutdown, over three quarters (77%) of respondents feel they are able to complete their work, and even though half (50%) of respondents claim an increased workload, two-thirds (65%) are satisfied with their current working conditions, with 45% saying they actually enjoy the new requirement of working from home.

Is It Time for a Job Change?

Despite all the workplace disruptions—or perhaps because of it—our survey results indicate that just four in ten respondents (44%) are not interested in seeking a job change. Generally, these respondents want to keep their current positions because of their current salary, or because of the location of their office and laboratories. Other reasons for staying put in current jobs are good work team colleagues, good management, and high competition for job positions. The same percentage (44%) would not want to leave their current position even if another promising job opportunity were presented.

On the other hand, a little over one-third of respondents (35%) would leave their current positions for a new or better opportunity. A full 26% indicated they were ready for a career change—either major or minor. According to respondents, the main general reasons for seeking new opportunities are higher salary, seeking new challenges, or dissatisfaction with their current

TABLE I: Average reported base salaries in USD from 2001 to 2020 (all respondents)

Survey Year	Average Salary (USD)	Percent Change vs Previous Year
2001	\$64,690 (first year)	NA
2002	\$67,900	5.0%
2003	\$68,180	0.4%
2004	\$72,140	5.8%
2005	\$72,920	1.1%
2006	\$77,980	6.9%
2007	\$79,605	2.1%
2008	\$77,364	-2.8%
2009	\$78,807	1.9%
2010	\$80,778	2.5%
2011	\$84,511	4.6%
2012	\$85,060	0.6%
2013	\$88,018	3.5%
2014	\$88,342	0.4%
2015	\$83,209	-5.8%
2016	\$82,457	-0.9%
2017	\$84,718	2.7%
2018	\$91,129	7.6%
2019	\$79,711	-12.5%
2020	\$86,491	8.5%
2021	\$88,025	1.8%

TABLE II: Number of years working in a career associated as a spectroscopist

No. of Years	%
Fewer than 5	3.74%
5–9	14.95%
10–15	21.50%
16–20	10.28%
21–35	33.64%
36–40	11.21%
41+	4.67%

employer. Some respondents have expressed that they are seeking new employment for mostly personal reasons (Figures 1a–1c).

Of course, thoughts about job change are often linked to perceptions of both job security and the strength of the job market. One in four respondents (25%) feel their jobs are less secure this year than last year, while about the same number (24%) feel they are

more secure; the rest (51%) say there is no change in their job security. Figure 2 displays the respondent perception of their current job security—an essential aspect of job satisfaction.

Almost half of survey respondents (55%) believe that the current employment market for spectroscopists is either good or excellent, and only 6% think it is poor. One in seven (15%) assess the job market as one where em-

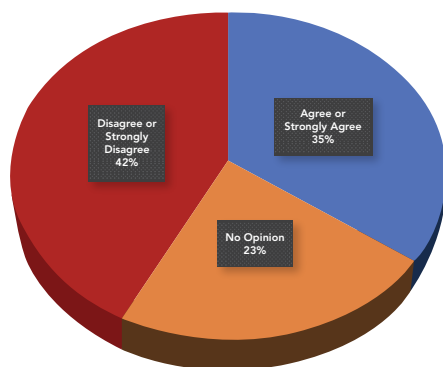


FIGURE 1A: Breakdown of desire to leave one's current job. The question was, "I would like to leave my current job if a new suitable opportunity presented itself."

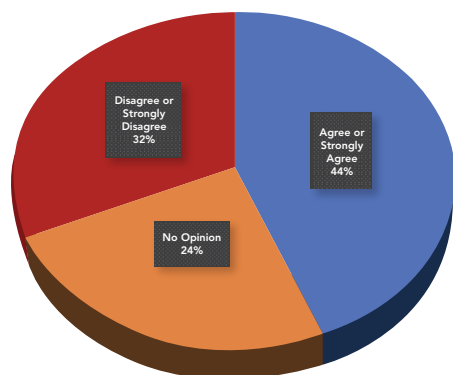


FIGURE 1B: Breakdown of desire to leave one's current job. The question was, "I do not want to leave my current position even if another opportunity was presented."

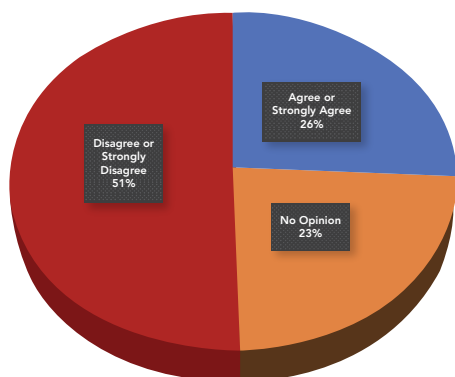


FIGURE 1C: Breakdown of desire to leave one's current job. The question was, "I am interested in changing careers."

ployer organizations are competing for good candidates, while the rest feel that there is moderate (55%) or strong (30%) competition from candidates for any acceptable open career positions (Figure 3).

What Factors Are Most Important in a Job

The vast majority (95%) of respondents say that salary and bonus structure is the most important factor in their jobs. The survey results indicated that the next most important factors (in rank order) were job security (93%), the work team (88%), intellectual challenge (88%), the importance of their work (87%), work-life balance (87%), the quality of equipment and laboratory space (85%), retirement benefits (82%), a tolerant work place (82%); and health insurance (79%). Those factors ranking lowest in importance for job satisfaction were maternity or paternity leave (27%)—not important to an older demographic—the prestige of the organization (39%), the ability to work from home (48%)—not a factor this year—and continued training and education (62%).

Salary and Bonus Results for 2021

For 2021, 37% of respondents received raises, but the vast majority (63%) did not. Alarming, it was noted that 13% experienced a decrease in pay over this past year (Figure 4). In our 2020 survey (2), we found that 20% of respondents did not receive a raise, but for that year we did not record any salary cuts for full-time professionals.

Our questions about pay scales indicated that one in twenty (5%) are very satisfied with their pay, and feel their pay is at the higher end of the market value for their jobs. Nearly one-third (35%) feel they are paid fairly. A full 65%, however, feel that they are paid at the low end of the scale, or are paid below market value.

For this year's survey, we recorded salaries between \$15,000 and \$250,000 USD (a typical range for our surveys). The reported mean and median annual salaries for all respondents were

\$88,025 and \$85,000, respectively, indicating the reported salaries are similar to those reported over the past few years. We note that there was a 1.8% increase in average salary compared to last year. Table I displays the annual average salary trend since 2001 for all respondents (See also Figure 5).

Reported bonuses for the 2021 survey were higher for this year compared to those in recent years. Nearly one-half (47%) of respondents reported receiving an annual bonus (compared to 54% last year) and the bonus amounts ranged from \$250 to \$40,000. The mean and median bonus values for all respondents receiving bonuses were \$19,228 and \$11,685, respectively, compared to \$14,121 and \$11,000 last year.

Respondent Profile

Of the spectroscopy professionals from around the world that responded to this year's survey, which was fielded in January 2021, the respondents were 66.7% male and 33.3% female. Respondents were from industry (58.9%), academic institutions (23.4%), government or nationally funded laboratories (6.5%), the military (1.9%), and (9.4%) from other organizations, such as private laboratories, hospitals, and medical facilities.

The various job titles of respondents, in order of occurrence, include principal or senior scientist (26.9%), scientist or associate (17.6%), manager (14.8%), full professor (8.3%), director (7.4%), technician (5.6%), CEO, CTO, or president (4.6%), associate or assistant professor (3.7%), laboratory assistant (1.9%), graduate student (1%), and other (8.3%). Note that 87% of respondents are full-time employees, while almost 5% are part-time employees, and nearly 2% are unemployed. Most respondents have a significant number of years of experience in spectroscopic methods, with nearly half of survey respondents with over 20 years (Table II and Figure 6).

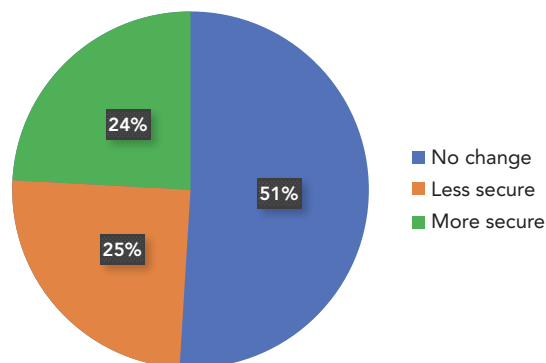


FIGURE 2: Perception of current job security. The survey question was, "How secure do you feel in your current position compared to last year?"

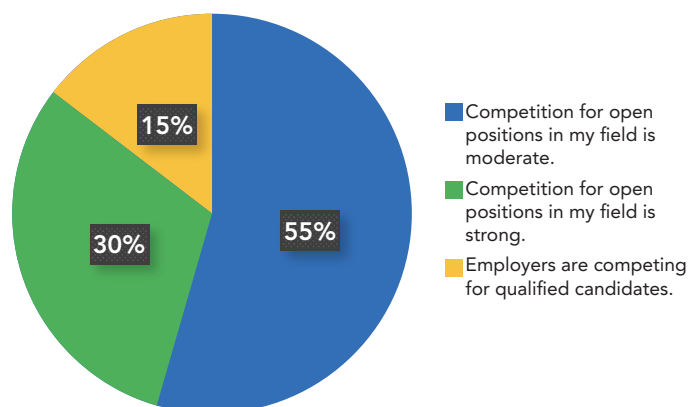


FIGURE 3: Strength of the job market for spectroscopists. The survey question was, "If it were necessary for you to change jobs this year, how would you assess the job market?"

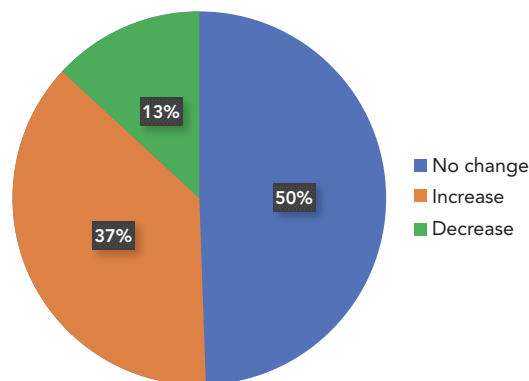


FIGURE 4: Overall change in salary during this past year. The question was, "What was the overall change in your salary during this past year?"

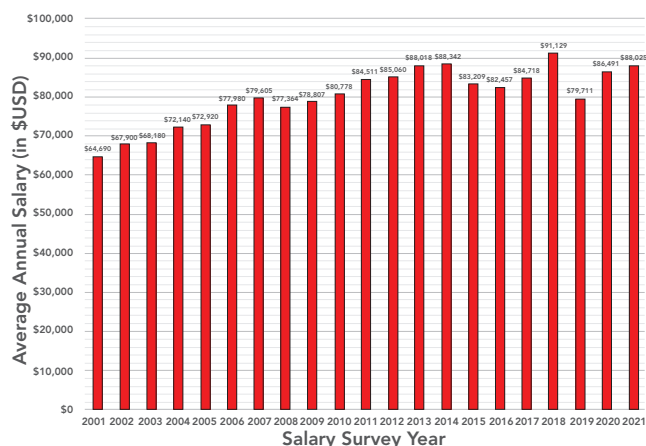


FIGURE 5: Reported average salaries for spectroscopy science professionals from 2001 through 2021 surveys (in \$USD).

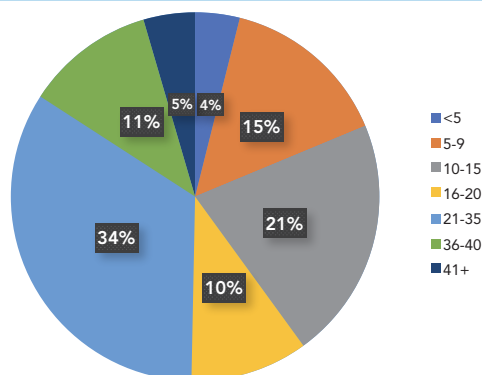


FIGURE 6: Number of years as a spectroscopist. The question was, “For how many years have you been working in a career connected with the spectroscopy field?”

Summary

Spectroscopy professionals across all fields working in 2020 through early 2021 have experienced unprecedented challenges and changes during this more than extraordinary year. Among our respondents, 13% experienced a pay cut this year—likely a result of Covid-19 shutdown issues—and 15% were either laid off or furloughed. Over half (51%) have limited or no access to their laboratories, and 34% say they are struggling to stay positive during this situation. In spite of all that, over three quarters (77%) of respondents feel they are able to complete their work despite the unusual challenges of this year.

They are also fairly optimistic about the coming year: Two-thirds of respondents expect the economy to recover in 2021, and the same number believe their job situation will improve during 2021. Our respondents also have strong confidence that their employers will have improved revenue in 2021 (60%).

Of course, the ongoing concerns related to any workplace remain, pandemic or not. We found that the greatest workplace concerns of professionals in the spectroscopy field are salary and bonus structure, job security, working colleagues and associates, intellectual challenge, the importance of the work, and work-life balance.

Almost two-thirds (65%) of spectroscopists reported they are satisfied with their current working conditions, even though half of respondents claim an increased workload. Just over one-third of our respondents indicate they are interested in seeking a better employment opportunity beyond their current situation.

We noted that just over one third of respondents received raises, while the remaining two-thirds did not—and 13% experienced a decrease in pay over this past year. A full two-thirds feel that they are either paid at the low end of the scale or are paid below market value. The mean and median annual salaries for the 2021 survey are similar to those in the recent past, with a slight increase for this year vs. the past two survey years (2019 and 2020 [1,2]).

All in all, 2021 will be remembered as an extremely challenging and confusing year. In spite of it all, professionals working in spectroscopy continue to remain positive, and to apply themselves and their skill sets to improve products, the environment, health research, and to advance the world of chemistry.

References

- (1) J. Workman, Jr., *Spectroscopy* **34**(3), 26–34 (2019).
- (2) J. Workman, Jr., *Spectroscopy* **35**(3), 39–50 (2020).



Jerome Workman, Jr. serves on the Editorial Advisory Board of *Spectroscopy* and is the Senior Technical

Editor for *LCGC* and *Spectroscopy*. He is also a Certified Core Adjunct Professor at U.S. National University in La Jolla, California. He was formerly the Executive Vice President of Research and Engineering for Unity Scientific and Process Sensors Corporation. Direct correspondence to jworkman@mjlifesciences.com •

Handheld Raman spectrometer

The NanoRam-1064 handheld Raman spectrometer from B&W Tek is designed for nondestructive identification and verification of raw materials such as active pharmaceutical ingredients, intermediates, and excipients. According to the company, the analyzer is suitable for the identification of colored samples, natural products, and for differentiating between different grades of cellulose, polysorbate, and Opadry.

B&W Tek, Newark, DE. www.bwtek.com



Atomic emission spectrometer

LECO's GDS900 glow discharge atomic emission spectrometer is designed for routine bulk elemental determination in most conductive solid metal matrices. According to the company, low melting alloys, resulfurized steel, powder metals, and other historically difficult-to-analyze materials can be analyzed in a production environment.

LECO Corporation, St. Joseph, MI.
<https://www.leco.com/product/gds900e>



Diamond ATR accessory

The IRIS diamond attenuated total reflection (ATR) accessory from PIKE is designed for infrared (IR) sampling for powders, gels, liquids, solids, and more. According to the company, the accessory is suitable for research, QA/QC, and sample identification.

PIKE Technologies, Madison, WI.
www.piketech.com



AA Lamps

REFLEX Analytical's selection of hollow cathode lamps for atomic absorption (AA) spectroscopy complements its available series of tungsten lamps, deuterium lamps, xenon lamps, photoionization detector (PID) lamps, mercury, and mercury-xenon ultraviolet detector lamps. According to the company, a selection of more than 1000 lamps for AA and a variety of other instrumentation and equipment is available.

REFLEX Analytical Corporation, Ridgewood, NJ. reflexusa.com



Acid vapor cleaning system

Saville's VC Ultra acid vapor cleaning system is designed to use high-purity acid vapors to acid-clean up to 40 microwave digestion vessels and covers in a single run. According to the company, customized microwave vessel cleaning racks minimize handling and acid exposure, and pre-loaded cleaning profiles eliminate the need for method development.

Saville, Eden Prairie, MN.
www.saville.com



Extended-range Raman spectrometer

The WP 532 EXR extended-range Raman spectrometer from Wasatch Photonics is designed for simultaneous measurement of the fingerprint region and extended functional bands using 532 nm excitation. According to the company, applications include inorganic materials and measurement of gases such as hydrogen.

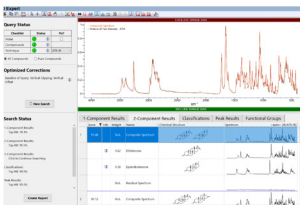
Wasatch Photonics, Morrisville, NC.
www.wasatchphotonics.com



Software and spectral databases

KnowItAll spectroscopy software by Wiley is designed to provide tools for spectroscopists to identify, analyze, verify, classify, and manage spectra. According to the company, its spectral library is the world's largest, containing more than two million spectra, including IR, MS, NIR, NMR, Raman, and UV-vis.

Wiley, Hoboken, NJ.
<https://sciencesolutions.wiley.com/spectral-databases/>



Automated microparticle analysis tool

Witec's ParticleScout automated microparticle analysis tool has been enhanced with features that include integration time optimization, vignetting correction, smart zoom, sample illumination options, smart separation of adjacent particles, and multiple sample area targeting. According to the company, the software provides for quantitative report formatting to present data using table, bar graph histogram, and pie chart templates.

Witec GmbH, Ulm, Germany. www.witec.de/particlescout/



PRODUCTS & RESOURCES

Palm spectrometer

The Breeze palm-held spectrometer from BaySpec is designed for 400–2500 nm with a one-button operation. According to the company, the spectrometer is suitable for the analysis of plastics, illicit drugs, pharmaceuticals, explosives, biological warfare agents, medicine, food, and other materials.

BaySpec Inc., San Jose, CA. www.bayspec.com



Particle analysis module

Renishaw's particle analysis software module for its inVia confocal Raman microscope is designed to automate the microscope so that it can identify particles on images, and then chemically analyze them using Raman spectroscopy. According to the company, the software provides chemical information on each particle and its morphology statistics.

Renishaw, West Dundee, IL. www.renishaw.com



CMOS camera

The Velocity Pro complementary metal-oxide semiconductor (CMOS) camera from EDAX is designed to provide highspeed electron backscatter diffraction (ESBD) mapping with high indexing performance on realworld materials. According to the company, the camera is powered by a CMOS sensor that is optimized for high-speed ESBD.

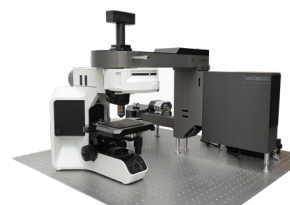
EDAX, Inc., Mahwah, NJ. www.edax.com



Raman microscope

The XperRAM S Raman microscope by Nanobase is designed to provide researchers with precise spectrum peak acquisition, wide area image scanning, and an easy-to-control software suite. According to the company, the microscope features a transmission spectrometer to increase spectrum peak efficiency to over 90%, and a wide and fast image scanning experience for over 200 μm x 200 μm .

Nanobase, Inc., Seoul, South Korea. www.nanobase.co.kr



AD INDEX

ADVERTISER

PG#

ABB.....	7
Analytik Jena AG.....	C4
B&W Tek.....	41
Bruker.....	18–19
Cannabis Science Conference.....	C3
CEM Corporation.....	15
LECO.....	11
Milestone Inc.....	37
Ocean Insight.....	C2

ADVERTISER

PG#

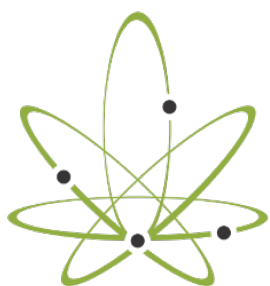
PIKE.....	5
REFLEX Analytical Corporation.....	29
Renishaw.....	8
Saville.....	39
Starna Cells, Inc.....	10,31
Wasatch Photonics.....	25
Wiley.....	3
WITec.....	17

BALTIMORE, MD

JUNE 28th – 30th

BALTIMORE CONVENTION CENTER

**THE WORLD'S LARGEST
CANNABIS SCIENCE EVENT!**



CANNABIS SCIENCE CONFERENCE



**ANALYTICAL, MEDICAL,
CULTIVATION & HEMP TRACKS**

Come grow with us!

- 125+ SPEAKERS
- EXCITING EXHIBITS
- CANNA BOOT CAMP
- PANEL DISCUSSIONS
- NETWORKING MIXERS
- CANNAQUARIUM EXPERIENCE

and much more!



The CSC Events team hopes that you are healthy and safe and we are excited to get our community back together in 2021. Now more than ever advancing science and medicine and sharing our research is needed and we look forward to seeing you again soon!

"Cannabis Science Conference has proven to be among the most influential educational events in the movement. They assemble the brightest researchers in the world to teach patients & medical professionals sitting side-by-side, learning together. Cannabis Science Conference is helping to galvanize rigorous scientific data supporting cannabis as a medicine."

- Sue Sisley, MD

- ! Sponsorship and exhibition opportunities are available.
- ! Please contact Andrea at Andrea@CannabisScienceConference.com for more info.

CannabisScienceConference.com



@CannabisScienceConference



@CannabisScienceConference

contrAA[®] 800

Atomic Absorption. Redefined



Atomic Absorption. Redefined. contrAA[®] 800

As a link between standard AAS instruments and ICP-OES spectrometers contrAA[®] 800 combines the best of two worlds: fast sequential and simultaneous multi-element analysis, ease of handling and manageable costs.

- **Multi Element:** One light source for fast sequential and simultaneous multi-element analysis
- **High-Resolution Optics:** Interference-free analysis and highest precision
- **HD Spectrum:** High-resolution 3D spectra display for detailed spectral information
- **Dynamic Mode:** Extended measurement range of up to 5 orders of magnitude

For more information, contact us:

info@us.analytik-jena.com
www.analytik-jena.us

30
years

analytikjena

An Endress+Hauser Company